The protective roles of Eugenol on type 1 diabetes mellitus through NRF2 mediated oxidative stress pathway

Yalan Jiang[a, 1], Pingping He[a, 1], Ke Sheng[b, 1], Yongmiao Peng[b], Huilan Wu[b], Songwei Qian[e], Weiping Ji[e, *], Xiaoling Guo[a, b, c,d, *], Xiaoou Shan[a, c, d,*]

[a]*Department of Pediatrics, the Second Affiliated Hospital and Yuying Children's Hospital of Wenzhou Medical University, Wenzhou, Zhejiang 325027, China*

[b]*Basic Medical Research Center, the Second Affiliated Hospital and Yuying Children's Hospital of Wenzhou Medical University, Wenzhou, Zhejiang 325027, China*

[c]*Key Laboratory of Children Genitourinary Diseases of Wenzhou, the Second Affiliated Hospital and Yuying Children's Hospital of Wenzhou Medical University, Wenzhou, Zhejiang 325027, China*

[d]*Key Laboratory of Structural Malformations in Children of Zhejiang Province, the Second Affiliated Hospital and Yuying Children's Hospital of Wenzhou Medical University, Wenzhou, Zhejiang 325027, China*

[e]*Department of General Surgery, the Second Affiliated Hospital and Yuying Children's Hospital of Wenzhou Medical University, Wenzhou, Zhejiang 325027, China*

**Correspondence: Weiping Ji, MD, Maoping Chu, MD, Xiaoling Guo, PhD, and Xiaoou Shan, MD, Basic Medical Research Center, the Second Affiliated Hospital and Yuying Children's Hospital of Wenzhou Medical University, 109 Xueyuan West Road, Wenzhou 325027, Zhejiang, China; Tel: 001-86-1375-886-0618; Fax: 86-0577-88002729; E-mail address: jiweiping@wmu.edu.cn, chmping@hotmail.com, guoxling@hotmail.com, Seagullshan@wmu.edu.cn.*

[1]*These authors contributed equally to this work.*

Formatted: Numbering: Continuous

Abstract

Type 1 diabetes mellitus (T1DM), known as insulin-dependent diabetes mellitus, is characterized by persistent hyperglycemia caused by damage to the pancreatic β cells and an absolute insulin deficiency, which will affect multiple organs and has a poor prognosis. Oxidative stress and apoptosis play a major role in the progression of T1DM. Eugenol (EUG) is a natural compound with anti-inflammatory, anti-oxidant, and anti-apoptosis activities. However, the potential effects of EUG on T1DM had not been investigated. In this study, we established the streptozotocin (STZ)-induced T1DM mouse model *in vivo* and STZ-induced pancreatic β cell MIN6 cell model *in vitro* to explore the protective effects of EUG on T1DM, and tried to illuminate the potential mechanism. Our results showed that EUG intervention could activate the expression of nuclear factor E2-related factor 2 (NRF2), increase the expressions of downstream proteins NQO-1 and HO-1 regulated by NRF2, alleviate pancreatic β cell damage in T1DM, elevate insulin secretion, and reduce the expression levels of apoptosis and oxidative stress related markers. Furthermore, these effects of EUG could be significantly reversed by ML385, an inhibitor of NRF2. The present study suggested that EUG exerted protective effects on pancreatic β cells in T1DM by mitigating apoptosis and oxidative stress through activating the NRF2 signaling pathway. Consequently, EUG holds great promise as a potential therapeutic candidate for T1DM.

Keywords: Type 1 diabetes (T1DM), Eugenol (EUG), Oxidative stress, Apoptosis, Pancreatic β cell, NRF2 signaling pathway

1. Introduction

Type 1 diabetes mellitus (T1DM) is a chronic and progressive autoimmune disease characterized by severe destruction of pancreatic β cells, resulting in absolute insulin insufficiency and subsequent hyperglycemia [1]. The symptoms of this disease are polydipsia, polyphagia, polyuria, wasting, etc., which can develop into ketoacidosis and even lead to death without any treatment [2]. Additionally, chronic hyperglycemia can cause various complications including diabetic nephropathy [3] and diabetic cardiomyopathy [4], imposing huge social and economic burdens. The global incidence of T1DM is rapidly increasing. According to the International Diabetes Federation (IDF), it is estimated that 537 million adults (20-79 years) worldwide were affected by diabetes in 2021, while more than 1.2 million children and adolescents (0-19 years) had T1DM. It is predicted that the number of individuals with diabetes will reach approximately 783 million worldwide by 2045, with developing countries experiencing the largest increase [5]. Currently, insulin intervention is the most effective way to treat T1DM, but there are still challenges on excessive fluctuations in blood glucose levels before and after meals [6] and life expectancy is shorter. Furthermore, in comparison to the general population, the quality of life is considerably compromised [7-9]. Therefore, it is crucial to explore more effective treatment strategies for T1DM patients.

Oxidative stress is a concept that has attracted much attention in recent years, which refers to the imbalance between the production of oxygen free radicals within cells and the attenuation of anti-oxidant reactions, and plays an important role in the pathogenesis of diabetes [10]. Hyperglycemia in diabetic patients can lead to increased production of reactive oxygen species (ROS) and expression of oxidative stress-related markers *in vivo*, while decreasing expression of anti-oxidant markers and disrupting internal homeostasis [11]. Normally, cells possess effective anti-oxidant protection mechanisms to maintain cell homeostasis, particularly through nuclear factor-E2-related factor 2 (NRF2), which serves as an efficient regulator of cellular anti-oxidant defense by modulating the expression of genes encoding anti-oxidant proteins [12]. NRF2 can bind to Kelch-like ECH-associated protein 1

(KEAP1) in the cytoplasm under normal physiological conditions, and then undergo degradation via ubiquitination. When cells are exposed to oxidative stress, NRF2 dissociates from KEAP1, avoids ubiquitination, and is transferred from the cytoplasm into the nucleus, where it subsequently enhances expression of target proteins such as NAD(P)H quinone oxidoreductase-1 (NQO-1) and heme oxygenase-1 (HO-1) by binding to the anti-oxidant response element (ARE) [13-17]. Furthermore, ROS can induce DNA damage, and alter the expression of proteins involved in cell regulation inhibition or activation, impairment of mitochondrial function, ultimately leading to apoptosis [18, 19]. Recent findings indicated that systemic activation of NRF2 signaling delays the onset of T1DM in spontaneous non-obese diabetic (NOD) mice models [20]. Therefore, targeting NRF2 may hold promise for T1DM prevention and treatment.

Eugenol (EUG), a phenolic aromatic compound, is obtained mainly from clove oil. It has various biological activities such as anti-oxidant, anti-inflammatory, anti-apoptotic, and anti-bacteria [21]. Previous study has demonstrated that EUG could reduce oxidative stress through activating the KEA1-NRF2 signaling pathway to alleviate colitis [22]. Additionally, EUG has been found to attenuate transmissible gastroenteritis virus-induced apoptosis through the ROS-NRF2-ARE signaling pathway [23].

So far, there has been no report to determine whether EUG has a protective effect on damaged pancreatic β cells in T1DM. Our study aims to investigate the protective effect of EUG on pancreatic β cell damage in streptozotocin (STZ)-induced T1DM mouse model and STZ-induced MIN6 cell model, and try to elucidate the underlying mechanism. The findings may provide a novel therapeutic candidate drug for T1DM.

2. Results

2.1 Eugenol (EUG) can relieve the symptoms associate with type 1 diabetes mellitus (T1DM) and reduce the blood glucose level in T1DM mice

The experimental design timeline for *in vivo* experiments was illustrated in Figure 1A. To evaluate the effects of EUG on T1DM mice, the fasting body weight (Figure 1B), the fasting blood glucose (Figure 1C), water intake in 24 h (Figure 1D), food intake in 24 h (Figure 1E), and area of urine-soaked pads in T1DM mice (Supplement Figure 1A) were recorded. The results showed that EUG effectively ameliorated the multiple symptoms associated with T1DM, including polydipsia, hyperphagia, polyuria, and weight loss, while 20 mg/kg EUG exhibited the most improvement. At the termination of the experiment, the mice in each group showed very different growth states (Supplement Figure 1B). The results showed that the mice in T1DM group were significantly smaller than mice in Control group, and EUG treatment could improve this phenomenon. Given that T1DM can elevate the levels of urinary glucose and urine ketone, we conducted biochemical analysis for urine glucose (Supplement Figure 1C) and urine ketone in each group of mice. The results (Figure 1F and 1G) showed that EUG administration exhibited a mitigating effect on the increase of urinary glucose and urine ketone caused by T1DM.

It is widely known that both oral glucose tolerance test (OGTT) and insulin tolerance tests (ITT) can be used to detect T1DM and predict prognosis [24, 25]. In this study, mice in each group were performed OGTT at week 1 (before T1DM induction), week 3 (one week after T1DM induction), week 5 (three weeks after T1DM induction), and week 10 (at the end of the experiment). The results demonstrated that EUG treatment could effectively decrease blood glucose levels and improve islet function in T1DM mice (Figure 1H and 1I). In addition, these findings were further demonstrated by the results of ITT (Figure 1J). Diabetes is a chronic progressive disease, and long-term elevated blood glucose can have harmful effects on vital organs such as the heart, kidneys, and liver [3, 4, 26] . Therefore, PAS staining was performed on the kidneys (Supplement Figure 1D). The results showed that T1DM indeed induced glycogen accumulation within the glomerulus, and EUG

intervention showed a significant reduction in such glycogen accumulation, thereby enhancing the prognosis of T1DM. In brief, EUG could relieve the symptoms and reduce the blood glucose level in T1DM mice.

2.2 EUG can improve the damage degree of islets in T1DM mice

Insulin is produced by the β cells of pancreatic islets. Western blot (Figure 2A) and RT-qPCR were employed to assess insulin expression levels in each group. The quantitative results of both western blot (Figure 2B) and RT-qPCR (Figure 2C) showed that there was a decrease in insulin expression in T1DM mice, while EUG intervention effectively increased insulin expression levels. In addition, the serum insulin levels of mice in each group were measured by ELISA at different time points. The results showed that serum insulin levels were significantly reduced after T1DM modeling, and subsequently recovered by EUG intervention as well as 20 mg/kg EUG exhibited the most improvement effect (Figure 2D). The hematoxylin and eosin (H&E) staining was performed to observe the structural integrity of the islets in each group of mice. The results showed that, in comparison to the Control group, the islet structure of T1DM mice exhibited severe damage with indistinct boundaries and evident vacuolization in the islet cells. EUG intervention could improve the damage degree of islets (Figure 2E). Furthermore, insulin immunohistochemical staining was performed to further assess insulin expression in each group of mice (Figure 2F). The quantitative result showed that EUG treatment significantly enhanced insulin expression in T1DM mice, and 20 mg/kg EUG displayed the most remarkable improvement (Figure 2G). These findings suggested that EUG intervention could effectively ameliorate islet damage in T1DM mice.

2.3 EUG can reduce the apoptosis of pancreatic β cells in T1DM mice

DNA is essential for cell survival, and γH2AX serves as a reliable marker for DNA damage [27]. Western blot was performed to assess the expression of γH2AX in each group of mice (Figure 3A). The results showed that the pancreatic β cells of T1DM mice had severe DNA damages, and EUG intervention could reduce the number of

DNA damages (Figure 3B). γH2AX immunohistochemical staining was also performed to assess γH2AX expression in each group of mice (Figure 3C). The quantitative results were consistent with those of western blot. It is well known that DNA damage in cells is closely associated with apoptosis (Figure 3D). To investigate the potential anti-apoptotic effects of EUG on mouse pancreatic β cells, western blot was conducted to evaluate the expression levels of BCL2, BAX, and Cleaved Caspase-3 in pancreatic β cells of mice in each group (Figure 4A). The results showed that there was a significant increase in the number of apoptotic pancreatic β cells in T1DM mice compared to Control group, and EUG intervention effectively inhibited the apoptosis of pancreatic β cells in T1DM mice as well as 20 mg/kg EUG had the most obvious effects (Figure 4B). Furthermore, the expression levels of *Bcl2* and *Bax* genes in pancreatic β cells of mice in each group were detected by RT-qPCR, and the results were consistent with those of western blot (Figure 4C). Finally, TUNEL staining was further performed to evaluate the apoptosis of pancreatic β cells in each group of mice (Figure 4D). The quantitative results showed an increased number of apoptotic pancreatic β cells in T1DM mice, which could be mitigated by EUG intervention (Figure 4E). These findings suggested that EUG exhibited a potential to attenuate pancreatic β cell apoptosis in T1DM mice.

2.4 EUG protects pancreatic β cells in T1DM mice by activating the NRF2 signaling pathway

Oxidative stress is a well-known pathogenic mechanism in T1DM [28]. In addition, EUG has been reported to have powerful anti-oxidant properties and can effectively activate nuclear factor E2-related factor 2 (NRF2) [29]. Western blot was used to detect the expression levels of total NRF2 protein (T-NRF2) and nuclear NRF2 protein (N-NRF2) in each group of mice (Figure 5A). The findings showed that compared to Control group, the T1DM group exhibited an up-regulation in NRF2 expression, and EUG intervention could effectively activate NRF2, exerting anti-oxidative effects (Figure 5B). The results of RT-qPCR were consistent with those of western blot (Figure 5C). Furthermore, western blot was conducted to evaluate the

expression of key proteins involved in the NRF2 signal pathway in each group of mice such as Kelch-like ECH-associated protein 1 (KEAP1), heme oxygenase-1 (HO-1), and NAD(P)H quinone dehydrogenase 1(NQO-1) (Figure 5D). The results showed that under the intervention of EUG, the protein expression levels of HO-1 and NQO-1 were increased, but the expression of KEAP1 was decreased due to the activation of NRF2 signaling pathway (Figure 5E). The result of *Ho-1* gene expression was consistent with those of the above protein expression (Figure 5F). Finally, biochemical assays were performed to detect the serum oxidative stress-related markers scuh as MDA, SOD, CAT, and GSH-Px in each group of mice. The oxidative stress related index (MDA) in the T1DM group was increased, and the expression of anti-oxidant stress related indexes (SOD, CAT, and GSH-Px) were significantly increased in EUG intervention group (Figure 5G). These data suggested that EUG could alleviate oxidative stress-induced pancreatic β cell damage in TIDM mice through activating NRF2 signaling pathway.

2.5 EUG can alleviate the impairment of streptozotocin (STZ)-induced MIN6 cells

To further explore the potential effects of EUG on T1DM, we established STZ-induced MIN6 cell model *in vitro*. The cytotoxicity of STZ on MIN6 cells was evaluated by CCK-8 assay. The results showed that the viability of MIN6 cells decreased in a dose-dependent manner after 24 h treatment with different concentrations of STZ (0-8 mM), and the optimal concentration for STZ treatment was 1 mM (Supplement Figure 2A). In addition, the cytotoxicity of EUG on MIN6 cells was also evaluated using CCK-8 assay. The results showed that EUG concentration in the range of 0-600 μM had no significant effect on cell viability (Supplement Figure 2B). Before 1 mM STZ treatment, MIN6 cells were treated with different concentrations of EUG (0-400 μM) for 2 h. The result showed that the viability of MIN6 cells was improved by EUG pre-treatment and reached the optimum after 50 μM EUG treatment (Supplement Figure 2C). Optical microscopy observation showed that compared to Control group, the number of cells in STZ group was significantly reduced and cell morphology was worse. EUG treatment

could alleviate the above phenomena, while the intervention of NRF2 inhibitor ML385 (10 μM) could aggravate the cell damage (Supplement Figure 2D).

Since pancreatic β cell damage can affect insulin secretion, we evaluated insulin protein and gene expression levels in different groups. Western blot (Figure 6A) and RT-qPCR were used to evaluate the expression levels of insulin protein and gene in each group. The results (Figure 6B and 6C) showed that insulin levels in the STZ-induced group were significantly lower than those in the Control group. However, after EUG treatment, STZ-induced insulin levels in MIN6 cells were significantly elevated, which could be reversed by the NRF2 inhibitor ML385 intervention. Furthermore, the cell culture supernatant of each group was collected for detecting insulin levels using ELISA, and the results were consistent with the above (Figure 6D). These findings suggested that EUG has the potential to enhance the insulin secretion of STZ-induced MIN6 cells.

2.6 EUG reduces STZ-induced MIN6 cell damage through activating the NRF2 signaling pathway

In order to further explore the potential mechanism of EUG on T1DM, ML385, the typical NRF2 antagonist, was used to assess the expression of NRF2 pathway related proteins by western blot (Figure 6E and 7A). The quantitative results showed that the protein levels of T-NRF2 and N-NRF2 in STZ-induced MIN6 cells were higher than those in the Control group, and EUG treatment markedly increased the expressions of T-NRF2 and N-NRF2 (Figure 6F). Furthermore, EUG treatment also elevated HO-1 and NQO-1 protein levels but reduced KEAP1 level (Figure 7B). However, ML385 could effectively reverse the effects of EUG on STZ-induced MIN6 cells. The quantitative results showed that the ratio of T-NRF2/β-Actin and N-NRF2/Lamin B decreased significantly after ML385 treatment, but EUG intervention could alleviate the decrease in NRF2 expression caused by ML385. Moreover, RT-qPCR (Figure 6G and 7C) and immunofluorescence staining (Figure 6H and 7D) were performed to assess the expressions of HO-1 and NRF2 in MIN6 cells with different treatments, and the trends of results were consistent with those of western blot (Figure 6I and 7E).

To further demonstrate that EUG can alleviate the STZ-induced MIN6 cells *in vitro* by activating the NRF2 signaling pathway, we used NRF2 inhibitor ML385 to detect oxidative stress in different groups. MitoSOX staining (Figure 7F) showed that EUG significantly reduced mitochondrial reactive oxygen species (ROS) levels in STZ-induced MIN6 cells, whereas ML385 could significantly weaken EUG effect (Figure 7G). These data suggested that EUG may ameliorate the damage of MIN6 cells caused by oxidative stress through activating NRF2 signaling pathway.

2.7 EUG inhibited STZ-induced apoptosis of islet β cell MIN6

To further demonstrate that EUG can alleviate STZ-induced MIN6 cell damage *in vitro* by activating the NRF2 signaling pathway, we used NRF2 inhibitor ML385 to evaluate the apoptosis of MIN6 cells with different treatments. Western blot result of γH2AX (Figure 8A) showed that STZ treatment increased the amount of DNA damage in MIN6 cells, while EUG intervention effectively reduced the amount of DNA damage in MIN6 cells, but ML385 intervention could reversed this phenomenon. The combination of EUG and ML385 exhibited a relatively weaker effect (Figure 8B). The results of γH2AX cell immunofluorescence staining (Figure 8C) were consistent with those of western blot (Figure 8D). Oxidative stress can lead to cell apoptosis [19]. Western blot (Figure 9A) was conducted to examine the expressions of apoptosis related proteins such as BCL2, BAX, and Cleaved Caspase-3, and the results showed that apoptosis was severe in STZ-induced MIN6 cells, while EUG intervention played an anti-apoptotic role and ML385 could reverse this phenomenon (Figure 9B). The RT-qPCR results of *Bcl2* and *Bax* were consistent with above findings (Figure 9C). In addition, TUNEL staining (Figure 9D) and flow cytometry (Figure 9F) were performed, and the trends of results were also consistent with the above results (Figure 9E and 9G).

Based on the above findings, we hypothesized that EUG possesses the ability to improve functional impairment of islet β cells in T1DM by reducing oxidative stress and apoptosis through activating the NRF2 signaling pathway. The potential mechanism of EUG in T1DM was depicted in Figure 10.

3. Discussion

Type 1 diabetes mellitus (T1DM) involves the destruction of pancreatic β cells, resulting in an absolute deficiency of insulin, and T1DM is more common among adolescents [1]. Although subcutaneous insulin injection is the standard clinical treatment for T1DM, it does not improve life quality of patients. Therefore, it is urgent to explore more effective treatments for T1DM. A large number of studies have demonstrated that oxidative stress and apoptosis play crucial roles in causing islet damage in T1DM [28, 30]. In this study, we aimed to investigate the protective effects of eugenol (EUG) on islet damage *in vivo* and *in vitro* T1DM models, and tried to illuminate the underlying mechanism.

EUG is a phenolic compound found in many aromatic plants, and possesses a range of pharmacological properties such as anti-oxidant, anti-inflammatory, anti-cancer, anti-bacteria, and so on [21]. EUG can reduce blood glucose levels, alleviate insulin resistance [31], inhibit the activity of key diabetes-related enzymes in diabetic rats [32], and inhibit the production of advanced glycosylation end products associated with diabetes [33]. Therefore, it is speculated that EUG may have a protective effect on diabetes. So far, there has been no studies confirming whether EUG has a protective effect on T1DM. In this study, we will try to explore the protective effects of EUG on streptozotocin (STZ)-induced *in vitro* and *in vivo* T1DM models. Our *in vivo* results showed that EUG administration could effectively ameliorate the T1DM symptoms such as polydipsia, polyphagia, polyuria, and weight loss, and also alleviate ketonuria and glycosuria of T1DM mice. In addition, due to EUG intervention, the islet damage of T1DM mice was mitigated, and the insulin secretion was enhanced as well as hyperglycemia symptom was also effectively alleviated. As a chronic disease, diabetes can affect multiple organs such as the kidney, liver, and heart [3, 4, 26]. In this study, PAS staining showed that EUG intervention could significantly reduce glomerular glycogen accumulation and improved the prognosis in T1DM mice. Our *In vitro* data showed that EUG treatment could ameliorate STZ-induced functional impairment of MIN6 cells and increase insulin secretion levels, while reducing apoptosis and reactive oxygen species (ROS)

production. Therefore, it can be speculated that EUG has the potential to treat T1DM.

The individuals suffering from diabetes exhibit chronic hyperglycemia, leading to the ROS generation that can cause cell damage through various mechanisms [34]. Mitochondria serve as the main source of ROS, and when mitochondrial dysfunction, there is an augmented ROS production in the mitochondrial respiratory chain [35]. The mitochondrial respiratory chain complex enzymes are impaired under persistent hyperglycemia, leading to the development of secondary complications in diabetes [36, 37]. Therefore, oxidative stress is widely recognized as a major factor in the pathogenesis of diabetes. Our study showed that MDA level was elevated in T1DM mice. This biomarker is associated with oxidative stress that represents the end product of lipid peroxidation caused by free radicals [38]. Additionally, anti-oxidant enzymes SOD, CAT, and GSH-Px can induce catabolism of superoxide and peroxides to protect the body from oxidative stress damage. In our study, there was a reduction in the levels of SOD, CAT, and GSH-Px in T1DM group *in vivo*, while EUG intervention could inhibit MDA level and promote productions of SOD, CAT, and GSH-Px in T1DM mice. These anti-oxidant enzymes subsequently inhibited oxidative stress response in T1DM mice by limiting free radical reaction. Mitochondria play a key role in the regulation of oxidative stress. MitoSOX fluorescence staining *in vitro* results showed that there was a significant increase in mitochondrial ROS in STZ-induced MIN6 cells, which could be reversed by EUG intervention. Furthermore, both *in vivo* and *in vitro* findings revealed that EUG could enhance the relevant indicator expressions of NRF2 signaling pathway, which is associated with anti-oxidant stress response. To further verify the relationship between EUG and the NRF2 signaling pathway, the NRF2 specific inhibitor ML385 was used *in vitro* experiments [39]. Notably, ML385 could significantly abolish the effects of EUG. Therefore, we speculated that the activation of NRF2 signaling pathway might serve as a protective mechanism of EUG against STZ-induced T1DM.

NRF2 is a transcription factor that plays a crucial role in cellular response to oxidative stress by inducing the expression of various anti-oxidants [40], and its activity is regulated by the endogenous inhibitor KEAP1 [41]. NRF2 and KEAP1

constitute a conserved intracellular defense mechanism against oxidative stress. Normally, KEAP1-CUL3-E3 ubiquitin ligase can target the N-terminal Neh2 domain of NRF2, and then facilitates NRF2 ubiquitination, thereby maintaining low level of NRF2 [42]. In response to oxidative stress, specific cysteine residues in KEAP1 are modified to induce conformational changes in KEAP1-CUL3-E3 ubiquitin ligase, disrupting NRF2 ubiquitination and facilitating its translocation into the nucleus for heterodimerization with small MAF protein (sMAF). This complex then binds to anti-oxidant response elements (ARE) located in the promoter region of various cytoprotective genes to promote their transcription and induce the expression of a series of cell protective genes, such as NQO1, HO-1, SOD, CAT, GSH-Px, exerting an anti-oxidative stress role [43]. Previous study had demonstrated that EUG could attenuate transmissible gastroenteritis virus-induced oxidative stress and apoptosis through the ROS-NRF2-ARE signaling pathway [23]. In this study, both *in vivo* and *in vitro* data showed that EUG activated NRF2, enhanced its nuclear translocation, and induced the expression of cytoprotective proteins NQO-1 and HO-1. Furthermore, *in vivo* study showed that NRF2 regulated the levels of anti-oxidant enzymes such as SOD, CAT, and GSH-Px to inhibit free radical reactions to exert a protective effect on T1DM mice. Our *in vivo* results suggested that EUG has the potential to alleviate pancreatic β cell damage through activating the NRF2 pathway, thereby enhancing insulin secretion and improving the prognosis of T1DM. Meanwhile, ML385 intervention effectively counteracted the anti-oxidant and anti-apoptotic effects of EUG, leading to reduced NRF2 nuclear translocation and down-regulation of anti-oxidant oxidases. Therefore, we speculated that EUG might alleviate pancreatic β cell damage through activating the NRF2 signaling pathway.

Mitochondria are the main sites for cellular ROS production, and intracellular ROS can serve as signaling molecules to regulate physiological functions of the body. ROS accumulation caused by hyperglycemia can lead to decreased mitochondrial membrane potential and increased membrane permeability [44-46]. The apoptotic factor cytochrome C (Cyct) is released into the cytoplasm to activate the Caspase cascade (e.g. Caspase9 and Caspase3 are activated successively), resulting in

chromosome aggregation and DNA fragmentation [47]. The protein Caspase-3, which is essential for cellular function, plays a pivotal role in the intricate process of programmed cell death known as apoptosis. The BCL-2 family proteins, including anti-apoptotic proteins such as BCL-2, BCL-xl, and pro-apoptotic proteins such as BAX and BAD, can regulate this process [48]. The dysregulation of the BCL2/BAX, characterized by aberrant expression of anti-apoptotic or pro-apoptotic genes, can initiate apoptosis and ultimately lead to organ damage [49]. The development of T1DM is caused by autoimmune destruction of islet β cells, and islet activation stimulates antigen-presenting cells to trigger the activation of $CD4^+$ helper T cells and subsequent the release of chemokines/cytokines [50, 51]. These cytokines then activate $CD8^+$ cytotoxic T cells, leading to the destruction of β cells. The apoptotic pathways of T1DM include exogenous (receptor mediated) and endogenous (mitochondria driven) mechanisms. Exogenous pathway encompasses $CD4^+$-$CD8^+$ interacting Fas pathway, while endogenous pathway involves a delicate balance between anti-apoptotic B-cell lymphoma (BCL-2) and BCL-xL proteins with pro-apoptotic Bax, Bad, Bid, and Bik proteins [52]. Therefore, targeted intervention of apoptosis can effectively improve the prognosis of T1DM. EUG has been reported to alleviate precancerous breast lesions by inhibiting apoptosis through the HER2/PI3K-AKT pathway [53]. In this study, our *in vivo* and *in vitro* results showed that EUG treatment significantly down-regulated the expression of BAX and Cleaved Caspase-3 but up-regulated the level of BCL2 in the T1DM mice, and reduced the number of TUNEL positive cells, exerting a protective effect on islet β cells in T1DM mice. Cell survival relies on DNA integrity, as any damage to DNA can trigger cell apoptosis or necrosis [27]. In this study, our data demonstrated that the expression of the DNA damage biomarker γH2AX was elevated in T1DM group *in vivo* and *in vitro*, but EUG intervention could reversed this trend. NRF2 can be involved in apoptosis regulation, and NRF2-deficient cells have increased spontaneous apoptosis [54]. Our *in vitro* results showed that the NRF2 specific inhibitor ML385 could decrease the anti-apoptosis effect of EUG on STZ-induced MIN6 cells. Therefore, we speculated that EUG could suppress apoptosis through activating the NRF2 signaling pathway.

In this study, *in vivo* and *in vitro* results suggested that EUG may play a protective role in pancreatic β cell damages of T1DM by alleviating oxidative stress and apoptosis via activating the NRF2 signaling pathway. However, there are certain limitations to our study. Firstly, ML385 was just used to assess the protective effect of EUG *in vitro* but not *in vivo*, and the inhibitory effect on NRF2 *in vivo* needs to be further investigated. Secondly, it is imperative to analyze the dynamics of NRF2 decay to determine whether EUG affects the stability of NRF2 protein and to further understand its mechanism of action. Lastly, although MIN6 cells are widely used in diabetes *in vitro* research, the primary islet cells would be optimal for T1DM study *in vitro*.

In conclusion, our studies demonstrated that EUG treatment could relieve the symptoms associate with T1DM and improve the damage of islets in T1DM mice. Moreover, EUG could suppress the impairment of STZ-induced MIN6 cell *in vitro*. EUG exhibits significant inhibitory effects on the oxidative stress and apoptosis in T1DM group *in vivo* and *in vitro* through activating the NRF2 mediated oxidative stress pathway. These findings suggested that EUG holds potential as a therapeutic option for patients with TIDM.

4. Material and methods

4.1 Animal

The male C57BL/6 mice with 18~20 g at the age of 5~6-weeks were purchased from Zhejiang Weitong Lihua Laboratory Animal Technology Co., LTD. The mice were housed in a temperature-controlled pathogen-free facility (SPF) environment with a light/dark cycle for 12 h, a temperature of 23°C ± 2°C, a relative humidity of 45%-55%, and free accessed to food and water. All experimental operations were approved by the Ethics Committee of Laboratory Animals of Wenzhou Medical University, and were strictly conducted in accordance with the Guide for the Care and Use of Laboratory Animals.

4.2 Animal experiment

After one week of adaptive feeding, type 1 diabetes mellitus (T1DM) mouse model was established by streptozotocin (STZ; Sigma-Aldrich, CA, USA)-induced C57BL/6 mice. In brief, after 5 h fasting each morning in each group of mice, STZ was dissolved in a 0.1 M sodium citrate buffer (Solarbio, China, Beijing), and then intraperitoneally injected into mice at a dose of 50 mg/kg for 5 consecutive days [55]. Due to the instability and photosensitivity of STZ solution, it was prepared under dark condition and used immediately. To prevent death from transient hypoglycemia, the mice were given the 10% glucose solution instead of water during T1DM modeling. Fasting blood glucose levels were measured three days after modeling, and mice with fasting glucose levels more than 250 mg/dL were included in the study.

Regarding eugenol (EUG; purity > 98%, MedChemExpress, NJ, USA) dosage setting, previous studies have demonstrated that oral administration of EUG (20mg/kg/day) is effective in improving hyperglycemic symptoms in mice for 15 weeks [56]. Additionally, studies have shown that oral administration of EUG (5, 10 mg/kg/day) can cure visceral leishmaniasis in mice [57]. Based on these reports, the T1DM mice in our study were divided into five groups, such as Control (n = 30), T1DM (n = 30), T1DM + EUG (5 mg/kg/day) (n = 30), T1DM + EUG (10 mg/kg/day) (n = 30), and T1DM + EUG (20 mg/kg/day) (n = 30). Each group received daily intragastric administration for 8 weeks, and Control group received an equal volume of normal saline. Fasting blood glucose levels and fasting weight were measured and recorded weekly. Finally, serum samples were collected through orbital blood collection technique, and pancreatic tissue were isolated for subsequent experiments.

4.3 Fasting blood glucose, oral glucose tolerance test (OGTT), and insulin tolerance test (ITT)

The oral glucose tolerance test (OGTT) and insulin tolerance test (ITT) are widely regarded as the criterion for diagnosing diabetes, and are crucial methods for assessing pancreatic islet function [24, 25]. After fasting for 14 h, the fasting blood glucose levels in each group mice were measured, and tail vein blood samples were collected and analyzed using a glucometer. OGTT was conducted in each group mice

by intragastric administering 20% glucose solution after fasting for 14 h, and blood glucose levels were measured at 0 min, 30 min, 60 min, 90 min, and 120 min after the first gavage administration. ITT was performed in each group mice by administering intraperitoneal injection of 0.75 U insulin/kg after fasting for 4 h and prepare 20% glucose solution to be administered in case a mouse became hypoglycemic. The blood glucose levels were measured at 0 min, 15 min, 30 min, 45 min, 60 min, and 90 min after the first intraperitoneal injection [58].

4.4 Food, water, urine volume, and urine glucose measurements

The changes in food and water intake for each group were recorded throughout the experiment by controlling the daily initial food intake (100g) and water quantity (250mL). The urine volume of each cage was measured by recording the area of the bedding material saturated with urine. The urine of mice in each group was collected to detect the urine glucose levels according to the Urine glucose Assay Kit (Jiancheng, Nanjing, Jiangsu, China).

4.5 Islet isolation

The method described by Xu et al. [59] was used to isolate islets. Firstly, the common bile duct was ligated, and collagenase V solution (0.8 mg/mL; Sigma-Aldrich, CA, USA) was retrograde injected through the common bile duct until the pancreas was filled and foliated. The pancreas was then digested in the same concentration of 5 mL collagenase V solution at 37℃ for 15 min until most of the pancreatic tissues were digested into chylous and silt. To stop digestion, 10 mL of 4℃ Hank's solution was added and then centrifuged after slight shaking, and stop immediately when the centrifugation speed reached 2000 rpm. The supernatant was discarded and the sediment was washed twice with Hanks balanced salt solution. Islet tissues were placed in 5 mL of 4℃ Ficoll density gradient medium (1.119). After mixing, a sequence of slow drips consisting of 2 mL 4℃ Ficoll density gradient medium (1.077) and 2 mL Hank's solution were added into the tube before centrifugation at 2000 rpm for 5 min. The sediment was washed again with Hank's solution, and then was picked

under a dissecting microscope (Leica, Germany). The isolated islets were promptly utilized for subsequent experimental procedures.

4.6 Insulin and ketonuria enzyme-linked immunosorbent assay (ELISA)

After collecting the culture supernatant of MIN6 cells and mouse serum from each group, insulin levels in the samples were assessed using a commercially available ELISA assay kit (Boyun, Shanghai, China) in accordance with the manufacturer's protocol. The urine of mice in each group was collected to detect the ketonuria levels according to the commercially available ELISA assay kit (Boyun, Shanghai, China).

4.7 Periodic acid-schiff (PAS) staining

After dewaxing the paraffin sections, periodic acid-schiff (PAS) staining kit (Servicebio, Wuhan, China) was used to detect glomerular glycogen accumulation. These tissue sections were immersed in a 0.5% periodate solution for 15 min, and then stained with Schiff reagent for 30 min in dark. Finally, the nuclei of these tissue sections were stained with hematoxylin reagent. The images of paraffin sections were captured using an optical microscope (Nikon, Japan).

4.8 Hematoxylin and eosin (H&E) staining

The fresh pancreatic tissues from mice in each group were carefully separated and promptly fixed with 4% paraformaldehyde (PFA; Solarbio, Beijing, China). After dehydration for 24 h, they were embedded by paraffin and sliced into 5 μm. Afterwards, the paraffin sections of pancreas were stained with hematoxylin and eosin (H&E) staining kit (Servicebio, Wuhan, China), and the pathological changes of pancreatic islets were observed under an optical microscope.

4.9 Immunohistochemistry staining

After dewaxing, the peroxidase blockade agent (Zsbio, Beijing, China) was applied to the tissue surface at room temperature (RT) for 20 min. After 15 min of washing with PBS, sections were subjected to antigen repair by boiling for 2 min in a pressure

cooker containing 10 mM citrate acid buffer (pH 6.0, Solarbio, Beijing, China). Subsequently, 10% goat serum (Beyotime, Shanghai, China) was used to block antigen, and then the slides were incubated with primary antibodies (listed in Supplementary Table 1) overnight at 4℃. On the second day, these sections were incubated with goat anti-rabbit secondary antibody (1:2000, Affinity Biosciences) at 37℃ for 2 h, and then stained with 3, 3' -diaminobenzidine DAB solution (Zsbio, Beijing, China) and hematoxylin. The images of pancreatic paraffin sections were captured using an optical microscope.

4.10 Cell culture and treatment

The mouse pancreatic β cell line MIN6 was purchased from the American Type Culture Collection (ATCC, Manassas, VA, USA), and was cultured in Dulbecco's Modified Eagle Medium (DMEM; Gibco, United States) containing 1% penicillin/streptomycin (P/S; Gibco, CA, USA), 10% fetal bovine serum (FBS; Gibco, CA, USA), and 1% MEM NON-ESSENTIAL AMINO ACIDS SOLUTION (100×; NEAA, Gibco, USA) at a 37°C, 5% CO_2 incubator. The cells were passaged every three days.

The *in vitro* cell model of T1DM was induced by STZ. MIN6 cells were treated with different concentrations of STZ (0.5 mM, 1 mM, 2 mM, 4 mM, and 8 mM) for 24 h to explore the optimal working concentration. Subsequently, STZ-induced MIN6 cells were treated with EUG at different concentrations (50 μM, 100 μM, 200 μM, 400 μM, and 600 μM) for 2 h to explore the optimal working concentration. Based on the optimal working concentrations of STZ and EUG, we set different groups such as Control, STZ, STZ + EUG, STZ + ML385 (10 μM, MedChemExpress, NJ, USA), STZ + ML385 + EUG. EUG or ML385 was pre-treated 2 h before the STZ stimulation, ML385 and EUG mixture in the same time. Finally, the cells or cell supernatant from each group were collected for subsequent experiments.

4.11 Cell viability assay

The cell viability of MIN6 cells with different treatments were assessed using the cell

counting kit-8 (CCK-8, Yeasen, Shanghai, China). MIN6 cells were seeded into 96-well plates at a density of 5×10^3/well. When reached 80%-90% confluence, the cells were treated with different concentrations of drugs. The different doses of EUG were added into the 96-well plates 2 h before STZ treatment. Following drug treatment, 100 μL DMEM containing 10 μL CCK-8 solution was added into each well. After incubation at 37℃ for 30 min, the absorbance of each well at 450 nm was measured using a microplate reader (Thermo Fisher Scientific, MA, USA).

4.12 Western blot

The total proteins from mouse islets or MIN6 cells were obtained using RIPA lysis buffer (Solarbio, Beijing, China) supplemented with a phosphatase inhibitor (Solarbio, Beijing, China) and a serine protease inhibitor (Solarbio, Beijing, China). Nuclear protein extraction kit (Beyotime, Shanghai, China) was used to extract nuclear proteins according to the manufacturer's instructions. Protein concentration was determined using BCA protein assay kit (Beyotime, Shanghai, China). The 7.5%, or 12.5% sodium dodecyl sulfate-polyacrylamide (SDS-PAGE) gels were employed to separate 20~80 μg proteins, which were subsequently transferred onto the polyvinylidene fluoride (PVDF) membranes (Thermo Fisher Scientific, MA, USA). These membranes were then blocked with 8% skim milk (Beyotime, Shanghai, China) at RT for 3 h. After washing with tris-buffered saline containing Tween-20 (TBST), these membranes were incubated overnight at 4℃ with primary antibodies listed in Supplementary Table 1. Then, these membranes were incubated with goat anti-mouse or goat anti-rabbit IgG HRP secondary antibodies (Affinity, Melbourne, Australia) diluted at a ratio of 1:5000 at RT for 3 h. Finally, the protein bands were detected using ECL chromogenic kit (EpiZyme, Shanghai, China), and visualized by ChemiDic™ XRS imaging system (Bio-Rad, CA USA). Image J software (National Institutes of Health, MD, USA) was used to analyze the intensity of protein bands which was normalized to β-Actin band.

4.13 Real–time quantitative polymerase chain reaction (RT–qPCR)

Total RNAs were extracted from mouse islets or MIN6 cells using Trizol reagent (Invitrogen, CA, USA). After measuring RNA concentration by reading OD value at 260 nm, RNAs were reverse-transcribed into cDNAs using cDNA Synthesis SuperMix (TaKaRa, Kusatsu, Japan), which were performed RT-qPCR using SYBR Green SuperMix (TOYOBO, Osaka, Japan). Then cycle threshold (Ct) values were collected and normalized to *β-actin* levels. The mRNA levels were calculated by the $2^{(-\Delta\Delta Ct)}$ method. The primer sequences are shown in Supplementary Table 2.

4.14 Immunofluorescence staining

MIN6 cells in different groups were fixed with 4% PFA for 20 min. Then, they were incubated with 0.3% Triton X-100 (Sigma-Aldrich, CA, USA) for 1 h, and followed by incubation with 10% goat serum. After rinsing with PBS three times, they were incubated overnight at 4℃ with the primary antibody (listed in Supplementary Table 1), and then incubated with FITC-conjugated goat anti-rabbit IgG secondary antibody (1:100; Earthox, LA, USA) for 2 h at RT. Afterwards, anti-fluorescence quencher containing DAPI was used to stain the nucleus. Finally, they were observed under a fluorescence microscope (Nikon, Tokyo, Japan).

4.15 TUNEL staining

In vivo experiments, pancreatic paraffin sections were first dewaxed in a 60°C oven, and then were incubated with protease K solution at 37°C for 30 min. After PBS rinsing, they were staining with TUNEL mixture (Roche, Basel, Switzerland) at 37°C for 1 h in dark. Then, they were performed DAB staining and hematoxylin staining. Finally, the images of these sections were captured under an optical microscope.

In vitro experiments, the apoptosis of MIN6 cells in each group was assessed using TUNEL apoptosis detection kit (Roche, Basel, Switzerland). Briefly, the cells were incubated with TUNEL reagent for 1 h at 37℃ in dark, and then were washed with PBS and stained with DAPI. Lastly, they were observed under a fluorescence microscope.

4.16 Annexin V and PI assay

Annexin V FITC/PI apoptosis detection kit (Becton Dickinson, NJ, USA) was used to detect apoptosis of MIN6 cells in different groups. Cells were collected and washed twice with 4℃ PBS before being resuspended in Binding Buffer. Subsequently, these cells were stained at RT with a mixture of 5 μL FITC Annexin V and 5 μL PI for 15 min in dark. Finally, the quantification of cell apoptosis ratio was detected using the Flow Cytometer (Beckman, CA, USA).

4.17 Mitochondrial reactive oxygen species (ROS) detection

Mitochondrial ROS levels were evaluated using the MitoSOX Red mitochondrial superoxide indicator (Yeasen, Shanghai, China). The reagent was diluted with dimethyl sulfoxide (DMSO, Solarbio, Beijing, China). Subsequently, the MIN6 cells in each experimental group were incubated with MitoSOX reagent for 30 min at 37°C in dark. Finally, the nucleus was stained with an anti-fluorescence quencher containing DAPI, and images were captured under a fluorescence microscope.

4.18 Statistical analysis

In this study, all data were expressed as mean ± SEM and analyzed by GraphPad Prism 9.0 (GraphPad Software Inc., CA, USA) and all experiments were repeated at least three times independently. Statistical significance was analyzed by Student's *t*-test or one-way ANOVA followed by Turkey's multiple comparisons. The criterion for statistical significance was set at a *p*-value of less than 0.05.

Disclosure statement

The authors affirm that they do not possess any identifiable conflicting financial interests.

Author contributions

Y.J. devised the experiments and conducted the majority of the study. Y.J. and X.G. drafted the manuscript. P.H. established the mice model and K.S. established the cell

culture system. Y.P., and H.W. prepared of reagents and materials. S.Q. analyzed the data. X.S., W.J., and X.G. contributed to critical revisions of the manuscript. The final manuscript has been reviewed and approved by all authors.

Funding

This work was supported by the Natural Science Foundation of Zhejiang Province (LY24H020008, LTGY23H030003, and TGY23H030014), the Major Science and Technology Special Project of Wenzhou (2018ZY018), the Public Welfare Science and Technology Plan Project of Wenzhou City (Y2020925 and Y20210174), and the Fourth Batch of Wenzhou Medical University 'Outstanding and Excellent Youth Training Project' (604090352/640).

Referrences:

[1] X. Lu, C. Zhao, Exercise and Type 1 Diabetes, Adv Exp Med Biol 1228 (2020) 107-121.

[2] F.Z. Syed, Type 1 Diabetes Mellitus, Ann Intern Med 175(3) (2022) Itc33-itc48.

[3] N. Papadopoulou-Marketou, S.A. Paschou, N. Marketos, S. Adamidi, S. Adamidis, C. Kanaka-Gantenbein, Diabetic nephropathy in type 1 diabetes, Minerva Med 109(3) (2018) 218-228.

[4] M. Wang, Y. Li, S. Li, J. Lv, Endothelial Dysfunction and Diabetic Cardiomyopathy, Front Endocrinol (Lausanne) 13 (2022) 851941.

[5] D.J. Magliano, E.J. Boyko, I.D.F.D.A.t.e.s. committee, IDF Diabetes Atlas, Idf diabetes atlas, International Diabetes Federation © International Diabetes Federation, 2021., Brussels, 2021.

[6] E. Cobry, K. McFann, L. Messer, V. Gage, B. VanderWel, L. Horton, H.P. Chase, Timing of meal insulin boluses to achieve optimal postprandial glycemic control in patients with type 1 diabetes, Diabetes Technol Ther 12(3) (2010) 173-7.

[7] E. Kalyva, E. Malakonaki, C. Eiser, D. Mamoulakis, Health-related quality of life (HRQoL) of children with type 1 diabetes mellitus (T1DM): self and parental perceptions, Pediatr Diabetes 12(1) (2011) 34-40.

[8] F.J. Cameron, C. Clarke, K. Hesketh, E.L. White, D.F. Boyce, V.L. Dalton, J. Cross, M. Brown, N.H. Thies, G. Pallas, P.W. Goss, G.A. Werther, Regional and urban Victorian diabetic youth: clinical and quality-of-life outcomes, J Paediatr Child Health 38(6) (2002) 593-6.

[9] R.G. Miller, A.M. Secrest, R.K. Sharma, T.J. Songer, T.J. Orchard, Improvements in the life expectancy of type 1 diabetes: the Pittsburgh Epidemiology of Diabetes Complications study cohort, Diabetes 61(11) (2012) 2987-92.

[10] J.L. Rains, S.K. Jain, Oxidative stress, insulin signaling, and diabetes, Free Radic Biol Med 50(5) (2011) 567-75.

[11] K. Maiese, S.D. Morhan, Z.Z. Chong, Oxidative stress biology and cell injury during type 1 and type 2 diabetes mellitus, Curr Neurovasc Res 4(1) (2007) 63-71.

[12] S. Sajadimajd, M. Khazaei, Oxidative Stress and Cancer: The Role of Nrf2, Curr Cancer Drug Targets 18(6) (2018) 538-557.

[13] A.T. Dinkova-Kostova, W.D. Holtzclaw, R.N. Cole, K. Itoh, N. Wakabayashi, Y. Katoh, M. Yamamoto, P. Talalay, Direct evidence that sulfhydryl groups of Keap1 are the sensors regulating induction of phase 2 enzymes that protect against carcinogens and oxidants, Proc Natl Acad Sci U S A 99(18) (2002) 11908-13.

[14] T. Nguyen, P. Nioi, C.B. Pickett, The Nrf2-antioxidant response element signaling pathway and its activation by oxidative stress, J Biol Chem 284(20) (2009) 13291-5.

[15] W.W. Wasserman, W.E. Fahl, Functional antioxidant responsive elements, Proc Natl Acad Sci U S A 94(10) (1997) 5361-6.

[16] D.D. Zhang, M. Hannink, Distinct cysteine residues in Keap1 are required for Keap1-dependent ubiquitination of Nrf2 and for stabilization of Nrf2 by chemopreventive agents and oxidative stress, Mol Cell Biol 23(22) (2003) 8137-51.

[17] H. Zhu, K. Itoh, M. Yamamoto, J.L. Zweier, Y. Li, Role of Nrf2 signaling in regulation of antioxidants and phase 2 enzymes in cardiac fibroblasts: protection against reactive oxygen and nitrogen species-induced cell injury, FEBS Lett 579(14) (2005) 3029-36.

[18] P.H. Aguiar, C. Furtado, B.M. Repolês, G.A. Ribeiro, I.C. Mendes, E.F. Peloso, F.R. Gadelha, A.M. Macedo, G.R. Franco, S.D. Pena, S.M. Teixeira, L.Q. Vieira, A.A.

Guarneri, L.O. Andrade, C.R. Machado, Oxidative stress and DNA lesions: the role of 8-oxoguanine lesions in Trypanosoma cruzi cell viability, PLoS Negl Trop Dis 7(6) (2013) e2279.

[19] M. Liu, X. Wu, Y. Cui, P. Liu, B. Xiao, X. Zhang, J. Zhang, Z. Sun, M. Song, B. Shao, Y. Li, Mitophagy and apoptosis mediated by ROS participate in AlCl(3)-induced MC3T3-E1 cell dysfunction, Food Chem Toxicol 155 (2021) 112388.

[20] Y. Yagishita, A. Uruno, D.V. Chartoumpekis, T.W. Kensler, M. Yamamoto, Nrf2 represses the onset of type 1 diabetes in non-obese diabetic mice, J Endocrinol (2019).

[21] M. Ulanowska, B. Olas, Biological Properties and Prospects for the Application of Eugenol-A Review, Int J Mol Sci 22(7) (2021).

[22] S. Chen, X. Wu, S. Tang, J. Yin, Z. Song, X. He, Y. Yin, Eugenol Alleviates Dextran Sulfate Sodium-Induced Colitis Independent of Intestinal Microbiota in Mice, J Agric Food Chem 69(36) (2021) 10506-10514.

[23] K. Wang, Y. Tang, X. Wu, H. Liang, D. Chen, B. Yu, J. He, X. Mao, Z. Huang, H. Yan, A. Wu, Y. Luo, P. Zheng, J. Yu, H. Wang, J. Luo, Eugenol Attenuates Transmissible Gastroenteritis Virus-Induced Oxidative Stress and Apoptosis Via ROS-NRF2-ARE Signaling, Antioxidants (Basel) 11(9) (2022).

[24] J.P.T. Guimarães, L.R. Filgueiras, J.O. Martins, S. Jancar, Leukotriene Involvement in the Insulin Receptor Pathway and Macrophage Profiles in Muscles from Type 1 Diabetic Mice, Mediators Inflamm 2019 (2019) 4596127.

[25] O. Helminen, S. Aspholm, T. Pokka, J. Ilonen, O. Simell, R. Veijola, M. Knip, OGTT and random plasma glucose in the prediction of type 1 diabetes and time to diagnosis, Diabetologia 58(8) (2015) 1787-96.

[26] J. Khoury, Y. Zohar, N. Shehadeh, T. Saadi, Glycogenic hepatopathy, Hepatobiliary Pancreat Dis Int 17(2) (2018) 113-118.

[27] A. Kinner, W. Wu, C. Staudt, G. Iliakis, Gamma-H2AX in recognition and signaling of DNA double-strand breaks in the context of chromatin, Nucleic Acids Res 36(17) (2008) 5678-94.

[28] J.D. Piganelli, M.J. Mamula, E.A. James, The Role of β Cell Stress and Neo-Epitopes in the Immunopathology of Type 1 Diabetes, Front Endocrinol

(Lausanne) 11 (2020) 624590.
[29] L. Ma, J. Liu, Q. Lin, Y. Gu, W. Yu, Eugenol protects cells against oxidative stress via Nrf2, Exp Ther Med 21(2) (2021) 107.
[30] I. Santin, D.L. Eizirik, Candidate genes for type 1 diabetes modulate pancreatic islet inflammation and β-cell apoptosis, Diabetes Obes Metab 15 Suppl 3 (2013) 71-81.
[31] B. Al-Trad, H. Alkhateeb, W. Alsmadi, M. Al-Zoubi, Eugenol ameliorates insulin resistance, oxidative stress and inflammation in high fat-diet/streptozotocin-induced diabetic rat, Life Sci 216 (2019) 183-188.
[32] K. Mnafgui, F. Kaanich, A. Derbali, K. Hamden, F. Derbali, S. Slama, N. Allouche, A. Elfeki, Inhibition of key enzymes related to diabetes and hypertension by Eugenol in vitro and in alloxan-induced diabetic rats, Arch Physiol Biochem 119(5) (2013) 225-33.
[33] P. Singh, R.H. Jayaramaiah, S.B. Agawane, G. Vannuruswamy, A.M. Korwar, A. Anand, V.S. Dhaygude, M.L. Shaikh, R.S. Joshi, R. Boppana, M.J. Kulkarni, H.V. Thulasiram, A.P. Giri, Potential Dual Role of Eugenol in Inhibiting Advanced Glycation End Products in Diabetes: Proteomic and Mechanistic Insights, Sci Rep 6 (2016) 18798.
[34] J. Chen, S.E. Stimpson, G.A. Fernandez-Bueno, C.E. Mathews, Mitochondrial Reactive Oxygen Species and Type 1 Diabetes, Antioxid Redox Signal 29(14) (2018) 1361-1372.
[35] S.R. Pieczenik, J. Neustadt, Mitochondrial dysfunction and molecular pathways of disease, Exp Mol Pathol 83(1) (2007) 84-92.
[36] A.J. Kowaltowski, N.C. de Souza-Pinto, R.F. Castilho, A.E. Vercesi, Mitochondria and reactive oxygen species, Free Radic Biol Med 47(4) (2009) 333-43.
[37] P. Jezek, L. Hlavatá, Mitochondria in homeostasis of reactive oxygen species in cell, tissues, and organism, Int J Biochem Cell Biol 37(12) (2005) 2478-503.
[38] A. Ayala, M.F. Muñoz, S. Argüelles, Lipid peroxidation: production, metabolism, and signaling mechanisms of malondialdehyde and 4-hydroxy-2-nonenal, Oxid Med Cell Longev 2014 (2014) 360438.
[39] A. Singh, S. Venkannagari, K.H. Oh, Y.Q. Zhang, J.M. Rohde, L. Liu, S. Nimmagadda, K. Sudini, K.R. Brimacombe, S. Gajghate, J. Ma, A. Wang, X. Xu, S.A.

Shahane, M. Xia, J. Woo, G.A. Mensah, Z. Wang, M. Ferrer, E. Gabrielson, Z. Li, F. Rastinejad, M. Shen, M.B. Boxer, S. Biswal, Small Molecule Inhibitor of NRF2 Selectively Intervenes Therapeutic Resistance in KEAP1-Deficient NSCLC Tumors, ACS Chem Biol 11(11) (2016) 3214-3225.

[40] Q.M. Chen, A.J. Maltagliati, Nrf2 at the heart of oxidative stress and cardiac protection, Physiol Genomics 50(2) (2018) 77-97.

[41] E. Kansanen, S.M. Kuosmanen, H. Leinonen, A.L. Levonen, The Keap1-Nrf2 pathway: Mechanisms of activation and dysregulation in cancer, Redox Biol 1(1) (2013) 45-9.

[42] P. Wang, J. Song, D. Ye, CRL3s: The BTB-CUL3-RING E3 Ubiquitin Ligases, Adv Exp Med Biol 1217 (2020) 211-223.

[43] C. Tonelli, I.I.C. Chio, D.A. Tuveson, Transcriptional Regulation by Nrf2, Antioxid Redox Signal 29(17) (2018) 1727-1745.

[44] H. Chen, X. Li, P.N. Epstein, MnSOD and catalase transgenes demonstrate that protection of islets from oxidative stress does not alter cytokine toxicity, Diabetes 54(5) (2005) 1437-46.

[45] D.A. Lepore, T.A. Shinkel, N. Fisicaro, T.B. Mysore, L.E. Johnson, A.J. d'Apice, P.J. Cowan, Enhanced expression of glutathione peroxidase protects islet beta cells from hypoxia-reoxygenation, Xenotransplantation 11(1) (2004) 53-9.

[46] L.I. Rachek, N.P. Thornley, V.I. Grishko, S.P. LeDoux, G.L. Wilson, Protection of INS-1 cells from free fatty acid-induced apoptosis by targeting hOGG1 to mitochondria, Diabetes 55(4) (2006) 1022-8.

[47] M. D'Amelio, V. Cavallucci, F. Cecconi, Neuronal caspase-3 signaling: not only cell death, Cell Death Differ 17(7) (2010) 1104-14.

[48] J.M. Adams, S. Cory, The Bcl-2 protein family: arbiters of cell survival, Science 281(5381) (1998) 1322-6.

[49] J. Liao, F. Yang, Z. Tang, W. Yu, Q. Han, L. Hu, Y. Li, J. Guo, J. Pan, F. Ma, X. Ma, Y. Lin, Inhibition of Caspase-1-dependent pyroptosis attenuates copper-induced apoptosis in chicken hepatocytes, Ecotoxicol Environ Saf 174 (2019) 110-119.

[50] S. Tsai, A. Shameli, P. Santamaria, CD8+ T cells in type 1 diabetes, Adv Immunol

100 (2008) 79-124.
[51] E.A. James, R. Mallone, S.C. Kent, T.P. DiLorenzo, T-Cell Epitopes and Neo-epitopes in Type 1 Diabetes: A Comprehensive Update and Reappraisal, Diabetes 69(7) (2020) 1311-1335.
[52] T. Tomita, Apoptosis of pancreatic β-cells in Type 1 diabetes, Bosn J Basic Med Sci 17(3) (2017) 183-193.
[53] M.L. Abdullah, O. Al-Shabanah, Z.K. Hassan, M.M. Hafez, Eugenol-Induced Autophagy and Apoptosis in Breast Cancer Cells via PI3K/AKT/FOXO3a Pathway Inhibition, Int J Mol Sci 22(17) (2021).
[54] A.A. Merchant, A. Singh, W. Matsui, S. Biswal, The redox-sensitive transcription factor Nrf2 regulates murine hematopoietic stem cell survival independently of ROS levels, Blood 118(25) (2011) 6572-9.
[55] B.L. Furman, Streptozotocin-Induced Diabetic Models in Mice and Rats, Curr Protoc 1(4) (2021) e78.
[56] K.J. Jeong, D.Y. Kim, H.Y. Quan, H.K. Jo, G.W. Kim, S.H. Chung, Effects of eugenol on hepatic glucose production and AMPK signaling pathway in hepatocytes and C57BL/6J mice, Fitoterapia 93 (2014) 150-62.
[57] M.R. Charan Raja, A. Kar, S. Srinivasan, D. Chellappan, J. Debnath, S. Kar Mahapatra, Oral administration of eugenol oleate cures experimental visceral leishmaniasis through cytokines abundance, Cytokine 145 (2021) 155301.
[58] C. Nagy, E. Einwallner, Study of In Vivo Glucose Metabolism in High-fat Diet-fed Mice Using Oral Glucose Tolerance Test (OGTT) and Insulin Tolerance Test (ITT), J Vis Exp (131) (2018).
[59] Y. Xu, H. Fu, Z. Wang, X. Zhou, Y. Xu, D. Wang, S. Xue, X. Li, [Improved methods of isolation and purification of rat islets and its viability research], Zhongguo Xiu Fu Chong Jian Wai Ke Za Zhi 24(4) (2010) 406-9.

Figure Legends

Figure. 1. The EUG treatment effectively alleviated symptoms associated with T1DM mice. (A) The schematic diagram depicts the progress of animal experiments

with EUG in STZ-induced T1DM mice. Different colors indicate different treatments for mice. (B) The fasting weight levels of mice was measured weekly in each group (n = 3). (C) The fasting blood glucose levels of mice was measured weekly in each group (n = 3). (D) The water intake/cage in each group of mice. (E) The food intake/cage in each group of mice. (F) Urine ketones in each group were detected by ELISA (n = 3). (G) The urine glucose levels of mice was measured by biochemical test in each group (n = 3). (H) The curve graph of oral glucose tolerance test (OGTT) from 0 min to 120 min at week 1, week 3, week 5, and week 10 (n = 3). (I) The quantitative results of OGTT at week 1, week 3, week 5, and week 10 (n = 3). (J) The curve graph of insulin tolerance test (ITT) from 0 min to 90 min at week 10 (n = 3). Mean ± SEM. $^{*}p < 0.05$, $^{**}p < 0.01$, $^{***}p < 0.001$ indicate significant differences, and *ns* > 0.05 means no significance difference.

Figure. 2. EUG improved the pancreas islet structure and function in T1DM mice. (A) The detection of Insulin expression in different groups using western blot. (B) The quantification of western blot gel bands in different groups (n = 3). (C) The gene levels of *Ins1* in different groups (n = 3). (D) ELISA analysis of serum fasting insulin levels at different time points (n = 3). (E) The representative H&E staining images of pancreatic paraffin sections in each group of mice. Scale bars 50 μm, 20 μm. (F) The representative immumohistochemical staining of Insulin in pancreas islet in each group of mice. Scale bars 50 μm, 20 μm. (G) The quantitative analysis of immumohistochemical staining (n = 3). Mean ± SEM. $^{*}p < 0.05$, $^{**}p < 0.01$, $^{***}p < 0.001$ indicate significant differences, and *ns* > 0.05 means no significance difference.

Figure. 3. EUG decreased the expression level of γH2AX in T1DM mice. (A) The detection of γH2AX expression in different groups using western blot. (B) The quantification of western blot gel bands in different groups (n = 3). (C) The representative immumohistochemical staining of γH2AX in pancreas islet in each group of mice. Scale bars 100 μm, 25 μm. (D) The quantitative analysis of immumohistochemical staining (n = 3). Mean ± SEM. $*p < 0.05$, $**p < 0.01$, $***p <$

0.001 indicate significant differences, and *ns* > 0.05 means no significance difference.

Figure. 4. EUG reduced apoptosis of pancreatic β cells in T1DM mice. (A) The detection of BCL2, BAX, Cleaved Caspase-3 expression in different groups using western blot. (B) The quantification of western blot gel bands in different groups (n = 3). (C) The gene levels of *Bax*, *Bcl2*, and *Bcl2/Bax* in different groups (n = 3). (D) The immumohistochemical staining of TUNEL in pancreas islet in each group of mice. Scale bars 50 μm, 20 μm. (E) The quantification results of TUNEL staining in different groups (n = 3). Mean ± SEM. $^{*}p < 0.05$, $^{**}p < 0.01$, $^{***}p < 0.001$ indicate significant differences, and *ns* > 0.05 means no significance difference.

Figure. 5. EUG attenuated excessive oxidative stress through activating NRF2 signaling pathway in T1DM mice. (A) The detection of T-NRF2, N-NRF2 expression in different groups using western blot. (B) The quantification of western blot gel bands in different groups (n = 3). (C) The gene levels of *Nrf2* in different groups (n = 3). (D) The detection of KEAP1, HO-1, and NQO-1 expression in different groups using western blot. (E) The quantification of western blot gel bands in different groups (n = 3). (F) The gene levels of *Ho-1* in different groups (n = 3). (G) The levels of serum biochemical indicators (MDA, SOD, CAT, and GSH-Px) in each group of mice. Mean ± SEM. $^{*}p < 0.05$, $^{**}p < 0.01$, $^{***}p < 0.001$ indicate significant differences, and *ns* > 0.05 means no significance difference.

Figure. 6. EUG improved STZ-induced MIN6 cells insulin secretion by facilitating NRF2 nuclear translocation *in vitro*. (A) The detection of Insulin expression in different groups using western blot. (B) The quantification of western blot gel bands in different groups (n = 3). (C) The gene levels of *Ins1* in different groups (n = 3). (D) ELISA analysis of serum insulin levels of MIN6 cell in different groups (n = 3). (E) The detection of T-NRF2, N-NRF2 expression in different groups using western blot. (F) The quantification of western blot gel bands in different groups (n = 3). (G) The gene levels of *Nrf2* in different groups (n = 3). (H) The

representative immunofluorescence staining images of NRF2 (green) in each group of MIN6 cells. Nuclei were stained with DAPI (blue). Scale bar 10 μm. (I) The quantification of immunofluorescence staining in different groups (n = 3). Mean ± SEM. $^{*}p < 0.05$, $^{**}p < 0.01$, $^{***}p < 0.001$ indicate significant differences, and *ns* > 0.05 means no significance difference.

Figure. 7. EUG promoted the expression of NRF2 signaling pathway related proteins to reduce intracellular ROS level. (A) The detection of KEAP1, HO-1, and NQO-1 expression in different groups using western blot. (B) The quantification of western blot gel bands in different groups (n = 3). (C) The gene levels of *Ho-1* in different groups (n = 3). (D) The representative immunofluorescence staining images of HO-1 (green) in each group of MIN6 cells. Nuclei were stained with DAPI (blue). Scale bar 10 μm. (E) The quantification of immunofluorescence staining in different groups (n = 3). (F) The generation of mitochondrial ROS in each group was detected by MitoSOX (red) and DAPI (blue) staining. Scale bar 100 μm. (G) The quantitative analysis of immunofluorescence staining in different groups (n = 3). Mean ± SEM. $^{*}p < 0.05$, $^{**}p < 0.01$, $^{***}p < 0.001$ indicate significant differences, and *ns* > 0.05 means no significance difference.

Figure. 8. EUG attenuated γH2AX expression in STZ-induced MIN6 cells *in vitro.* (A) The detection of γH2AX expression in different groups using western blot. (B) The quantification of western blot gel bands in different groups (n = 3). (C) The representative immunofluorescence staining images of γH2AX (red) in each group of MIN6 cells. Nuclei were stained with DAPI (blue). Scale bar 50 μm. (D) The quantitative analysis of γH2AX positive cells in different groups (n = 3) Mean ± SEM. $^{*}p < 0.05$, $^{**}p < 0.01$, $^{***}p < 0.001$ indicate significant differences, and *ns* > 0.05 means no significance difference.

Figure. 9. EUG exerted protection of STZ-induced MIN6 cells through inhibition of the apoptosis *in vitro*. (A) The detection of BCL2, BAX, Cleaved Caspase-3

expression in different groups using western blot. (B) The quantification of western blot gel bands in different groups (n = 3). (C) The gene levels of *Bax*, *Bcl2*,and *Bcl2/Bax* in different groups (n = 3). (D) The detection of MIN6 cells apoptosis in each group using TUNEL staining. The cells with red fluorescence represents apoptosis. Scale bar 100 μm. (E) The quantitative analysis of TUNEL positive cells in different groups (n = 3). (F) The apoptosis in each group was analyzed using flow cytometry after Annexin V FITC and PI co-staining. (G) The quantitative analysis of flow cytometry after Annexin V FITC and PI co-staining in different groups (n = 3). Mean ± SEM. $^{*}p < 0.05$, $^{**}p < 0.01$, $^{***}p < 0.001$ indicate significant differences, and *ns* > 0.05 means no significance difference.

Figure. 10. Diagram of the underlying mechanisms involved in the protective effects of EUG on T1DM.

Supplement Figure. 1. EUG alleviated the related complications in T1DM mice. (A) The changes of urine wetting area of bedding material of mice in each group at different time points were recorded. (B) External appearance and body transformation in each group of mice (n = 3). Scale bar 2 cm. (C) The qualitative determination of urine glucose in each group of mice (n = 3). The shade of orange represents the concentration of glucose in the urine. (D) The PAS staining images of glomerulus paraffin sections in each group of mice. Mean ± SEM. $^{*}p < 0.05$, $^{**}p < 0.01$, $^{***}p < 0.001$ indicate significant differences, and *ns* > 0.05 means no significance difference. Scale bars 50 μm, 20 μm.

Supplement Figure. 2. Explored the optimal concentration of drugs for MIN6 cells *in vitro*. (A) The cell viability of MIN6 treated with different dose STZ for 24 h using CCK-8 assay (n = 3). (B) The safe dose ranges of EUG to maintain cell viability was determined by CCK-8 assay (n = 3). (C) The dose-dependent effect of EUG on MIN6 cell viability after STZ-induced (n = 3). (D) The imaging results of MIN6 cells under an inverted microscope in bright field with different treatments. Mean ± SEM.

$^{*}p < 0.05$, $^{**}p < 0.01$, $^{***}p < 0.001$ indicate significant differences, and *ns* > 0.05 means no significance difference. Scale bars 100 µm.

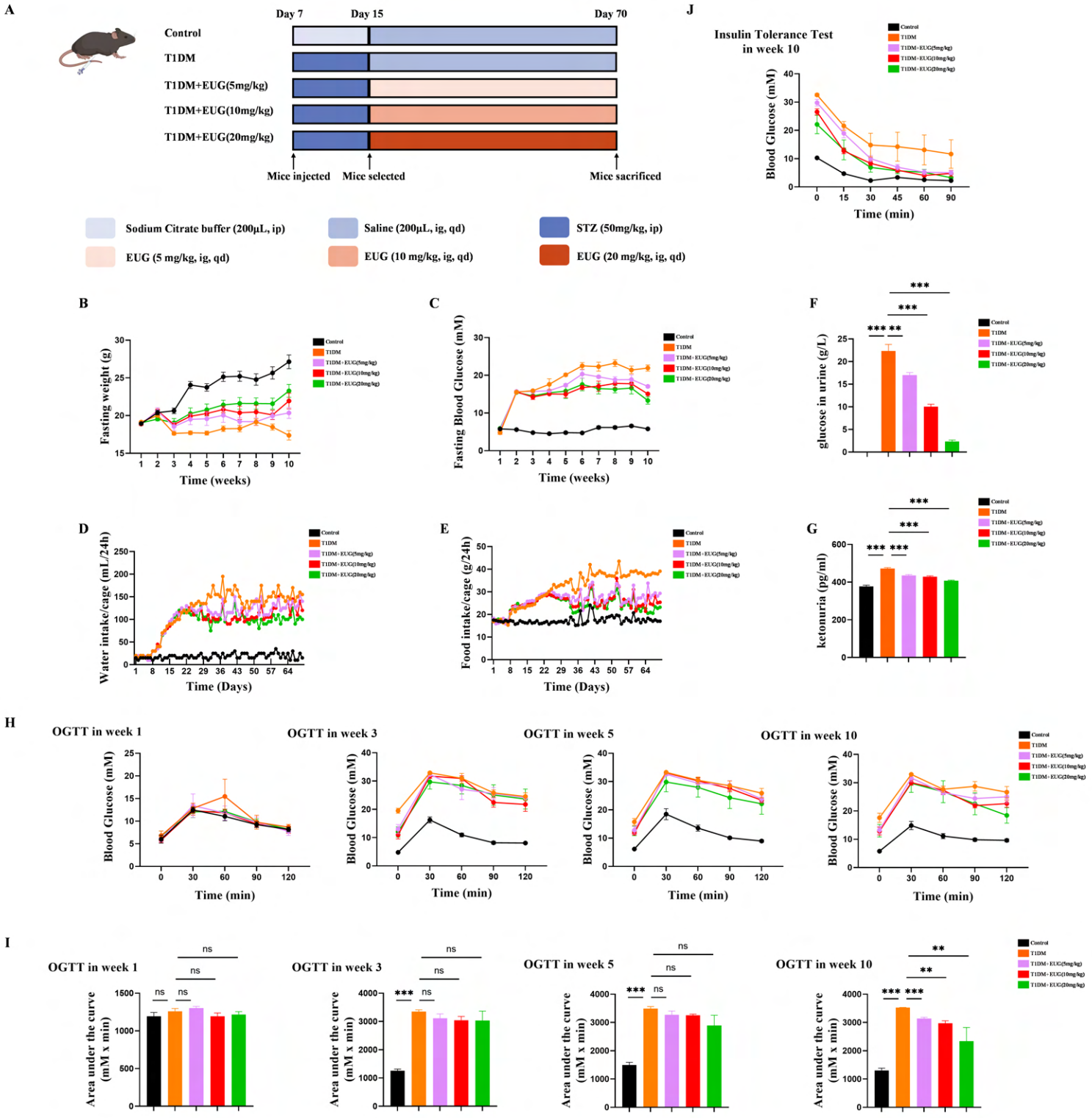
A
Day 7
Day 15
Day 70
Control
T1DM
T1DM+EUG(5mg/kg)
T1DM+EUG(10mg/kg)
T1DM+EUG(20mg/kg)
Mice injected
Mice selected
Mice sacrificed
Sodium Citrate buffer (200μL, ip)
Saline (200μL, ig, qd)
STZ (50mg/kg, ip)
EUG (5 mg/kg, ig, qd)
EUG (10 mg/kg, ig, qd)
EUG (20 mg/kg, ig, qd)
J
Insulin Tolerance Test in week 10
Blood Glucose (mM)
Time (min)
B
Fasting weight (g)
Time (weeks)
C
Fasting Blood Glucose (mM)
Time (weeks)
F
glucose in urine (g/L)
D
Water intake/cage (mL/24h)
Time (Days)
E
Food intake/cage (g/24h)
Time (Days)
G
ketonuria (pg/ml)
H
OGTT in week 1
OGTT in week 3
OGTT in week 5
OGTT in week 10
Blood Glucose (mM)
Time (min)
I
OGTT in week 1
OGTT in week 3
OGTT in week 5
OGTT in week 10
Area under the curve (mM x min)
ns
***
**

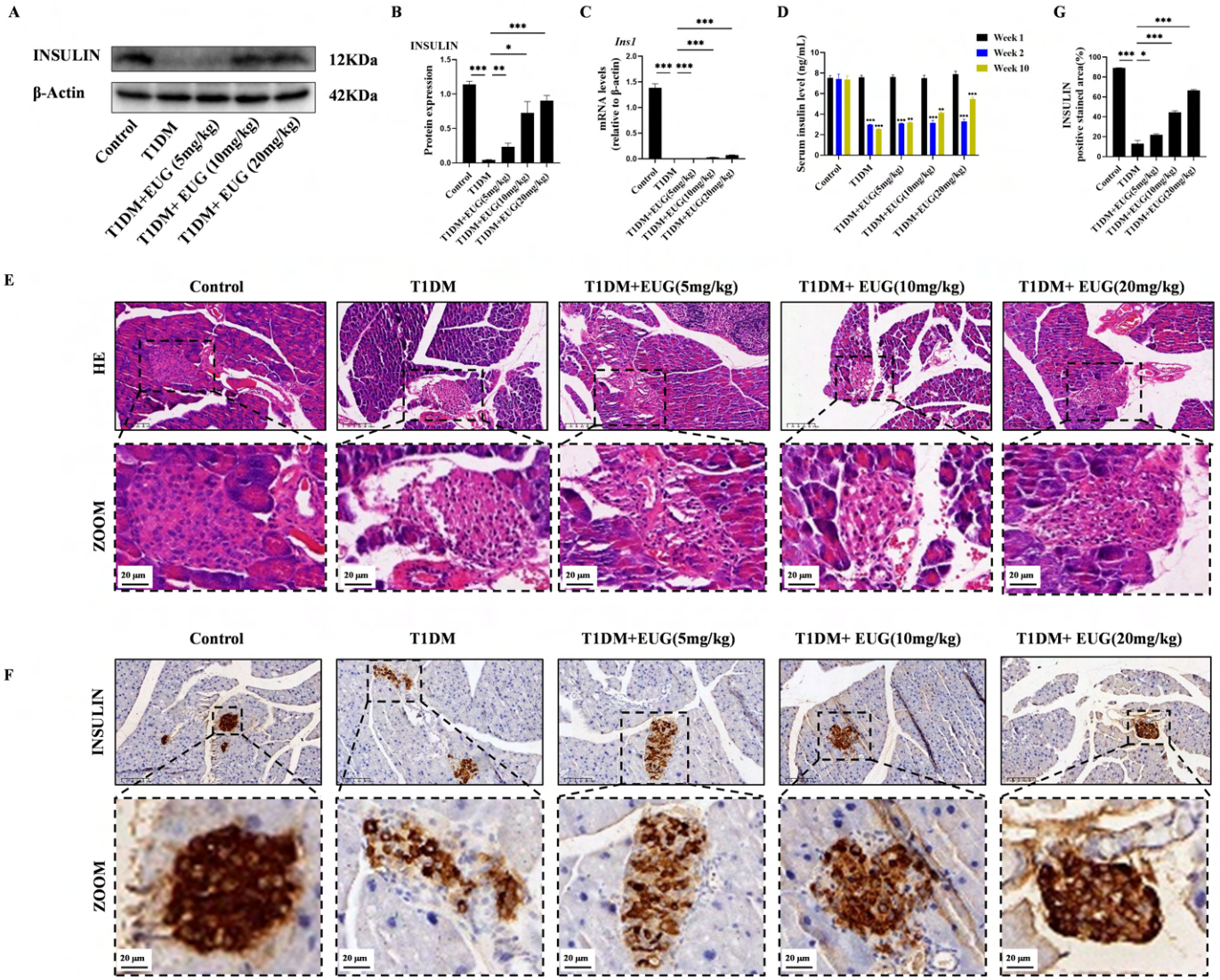
A
INSULIN
β-Actin
12KDa
42KDa
Control
T1DM
T1DM+EUG (5mg/kg)
T1DM+ EUG (10mg/kg)
T1DM+ EUG (20mg/kg)
B
INSULIN
Protein expression
C
Ins1
mRNA levels (relative to β-actin)
D
Serum insulin level (ng/mL)
Week 1
Week 2
Week 10
G
INSULIN positive stained area(%)
E
HE
ZOOM
20 μm
F
INSULIN
ZOOM
20 μm

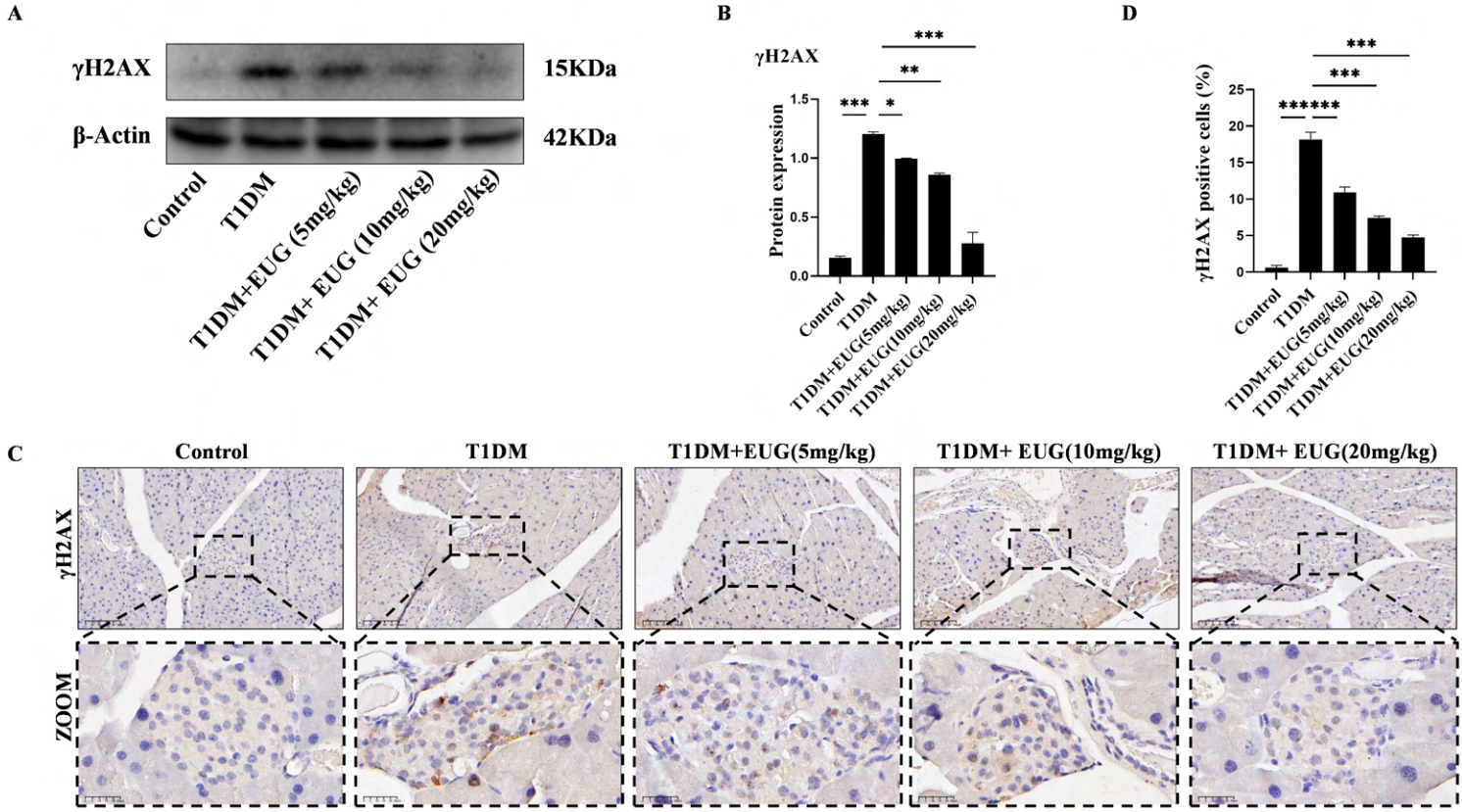
A
γH2AX
15KDa
β-Actin
42KDa
Control
T1DM
T1DM+EUG (5mg/kg)
T1DM+ EUG (10mg/kg)
T1DM+ EUG (20mg/kg)
B
γH2AX
Protein expression
1.5
1.0
0.5
0.0
***
*
**
***
Control
T1DM
T1DM+EUG(5mg/kg)
T1DM+EUG(10mg/kg)
T1DM+EUG(20mg/kg)
D
γH2AX positive cells (%)
25
20
15
10
5
0
******
***
***
Control
T1DM
T1DM+EUG(5mg/kg)
T1DM+EUG(10mg/kg)
T1DM+EUG(20mg/kg)
C
Control
T1DM
T1DM+EUG(5mg/kg)
T1DM+ EUG(10mg/kg)
T1DM+ EUG(20mg/kg)
γH2AX
ZOOM

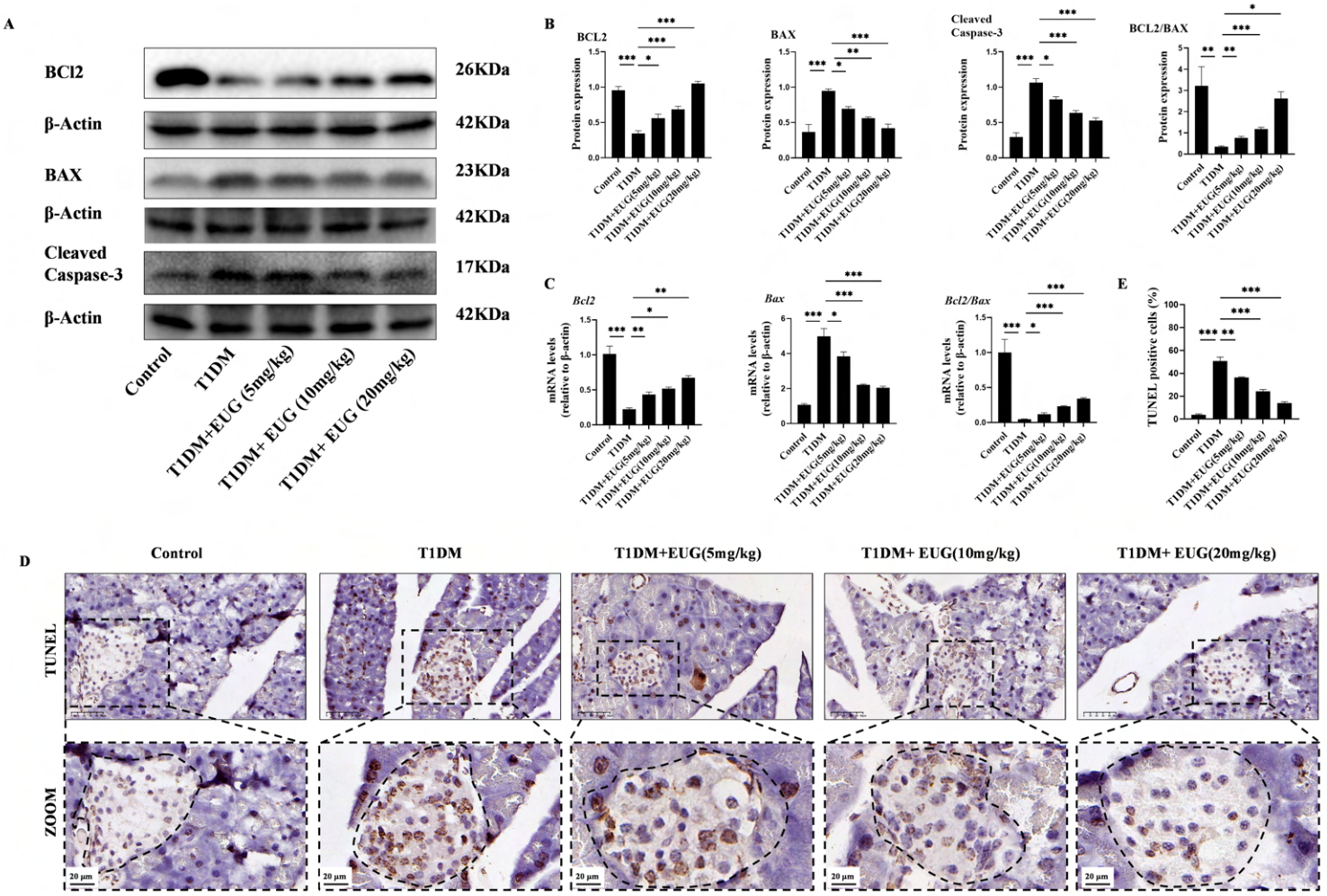
A
BCl2
26KDa
β-Actin
42KDa
BAX
23KDa
β-Actin
42KDa
Cleaved Caspase-3
17KDa
β-Actin
42KDa
Control
T1DM
T1DM+EUG (5mg/kg)
T1DM+ EUG (10mg/kg)
T1DM+ EUG (20mg/kg)
B
BCL2
BAX
Cleaved Caspase-3
BCL2/BAX
Protein expression
C
Bcl2
Bax
Bcl2/Bax
mRNA levels (relative to β-actin)
E
TUNEL positive cells (%)
D
Control
T1DM
T1DM+EUG(5mg/kg)
T1DM+ EUG(10mg/kg)
T1DM+ EUG(20mg/kg)
TUNEL
ZOOM
20 μm

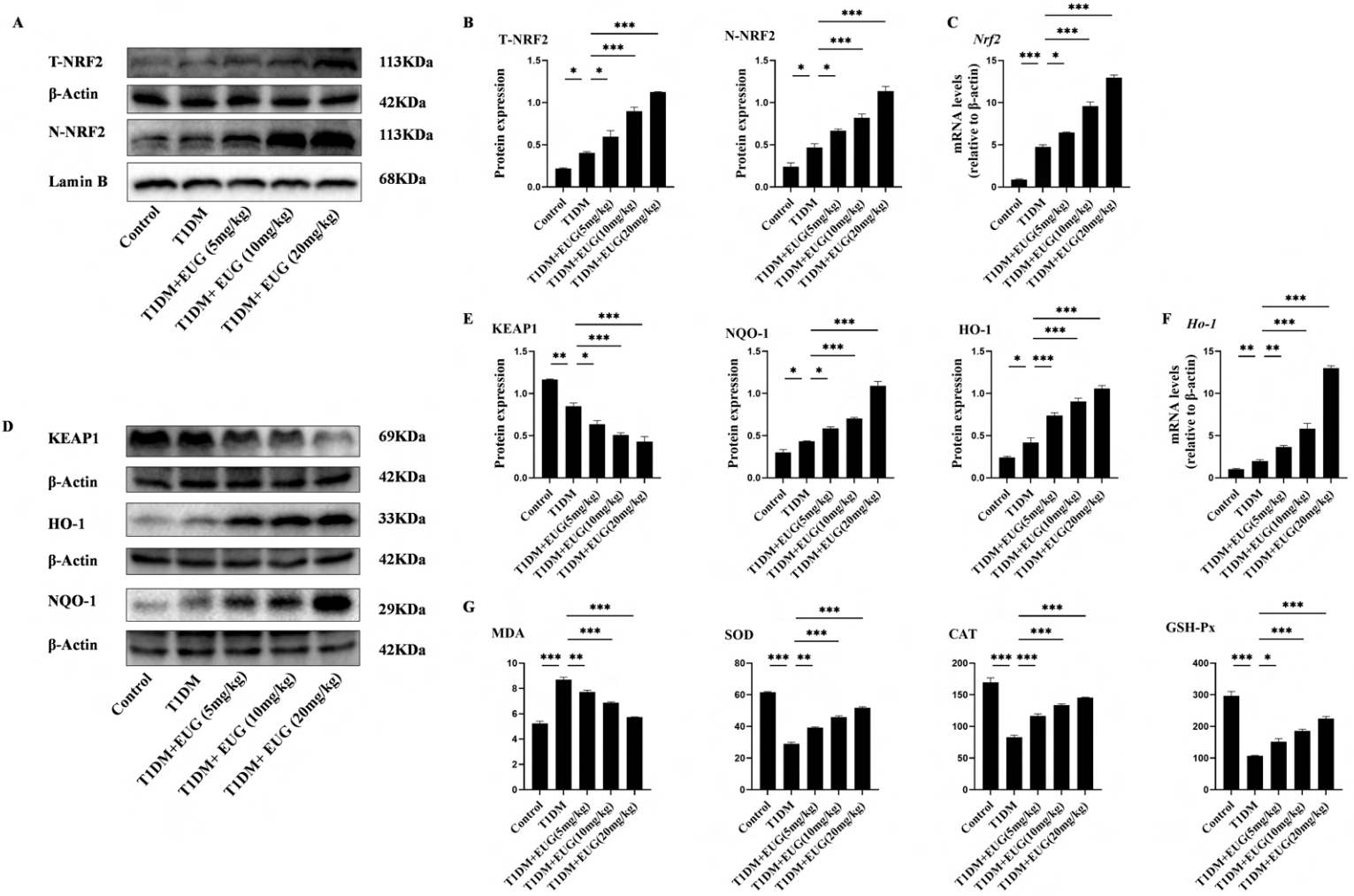
A
T-NRF2
β-Actin
N-NRF2
Lamin B
113KDa
42KDa
113KDa
68KDa
Control
T1DM
T1DM+EUG (5mg/kg)
T1DM+ EUG (10mg/kg)
T1DM+ EUG (20mg/kg)
B
T-NRF2
N-NRF2
Protein expression
C
Nrf2
mRNA levels (relative to β-actin)
D
KEAP1
β-Actin
HO-1
NQO-1
69KDa
42KDa
33KDa
29KDa
E
KEAP1
NQO-1
HO-1
F
Ho-1
G
MDA
SOD
CAT
GSH-Px

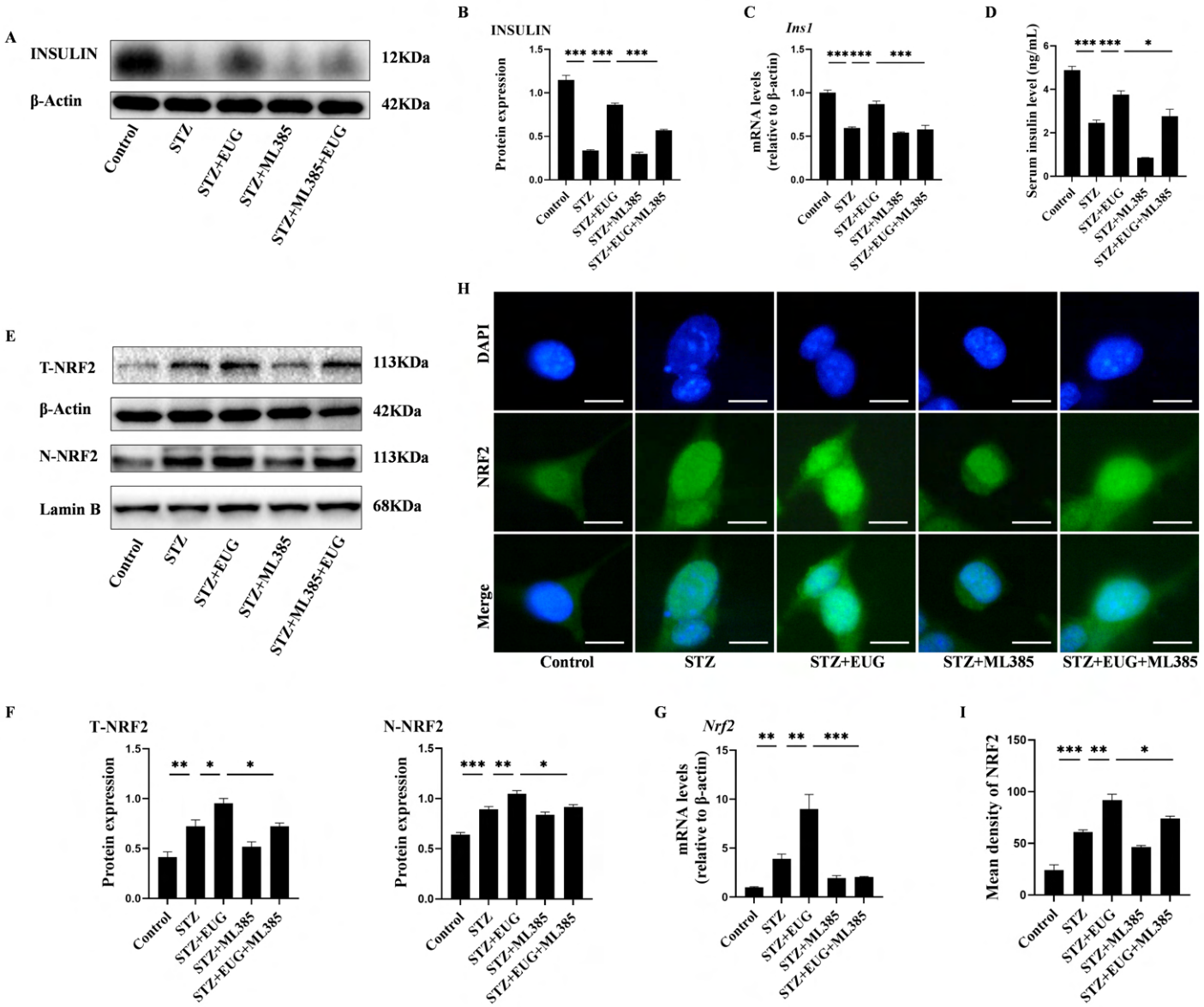
A
INSULIN
β-Actin
12KDa
42KDa
Control
STZ
STZ+EUG
STZ+ML385
STZ+ML385+EUG
B
INSULIN
Protein expression
C
Ins1
mRNA levels (relative to β-actin)
D
Serum insulin level (ng/mL)
E
T-NRF2
β-Actin
N-NRF2
Lamin B
113KDa
42KDa
113KDa
68KDa
H
DAPI
NRF2
Merge
Control
STZ
STZ+EUG
STZ+ML385
STZ+EUG+ML385
F
T-NRF2
N-NRF2
Protein expression
G
Nrf2
mRNA levels (relative to β-actin)
I
Mean density of NRF2

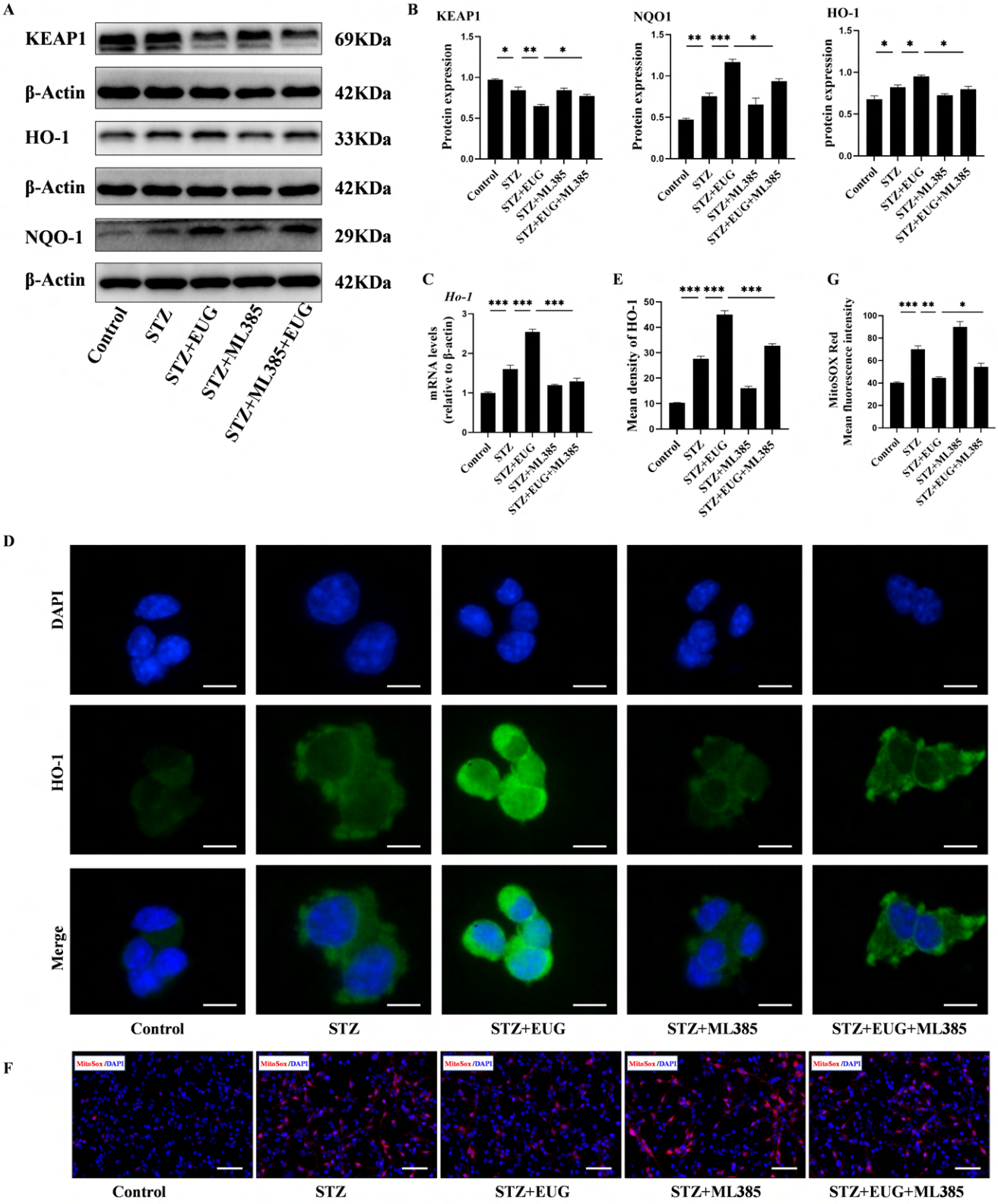
A
KEAP1
69KDa
β-Actin
42KDa
HO-1
33KDa
β-Actin
42KDa
NQO-1
29KDa
β-Actin
42KDa
Control
STZ
STZ+EUG
STZ+ML385
STZ+ML385+EUG
B
KEAP1
Protein expression
NQO1
Protein expression
HO-1
protein expression
Control
STZ
STZ+EUG
STZ+ML385
STZ+EUG+ML385
C
Ho-1
mRNA levels (relative to β-actin)
E
Mean density of HO-1
G
MitoSOX Red Mean fluorescence intensity
D
DAPI
HO-1
Merge
Control
STZ
STZ+EUG
STZ+ML385
STZ+EUG+ML385
F
MitoSox /DAPI
Control
STZ
STZ+EUG
STZ+ML385
STZ+EUG+ML385

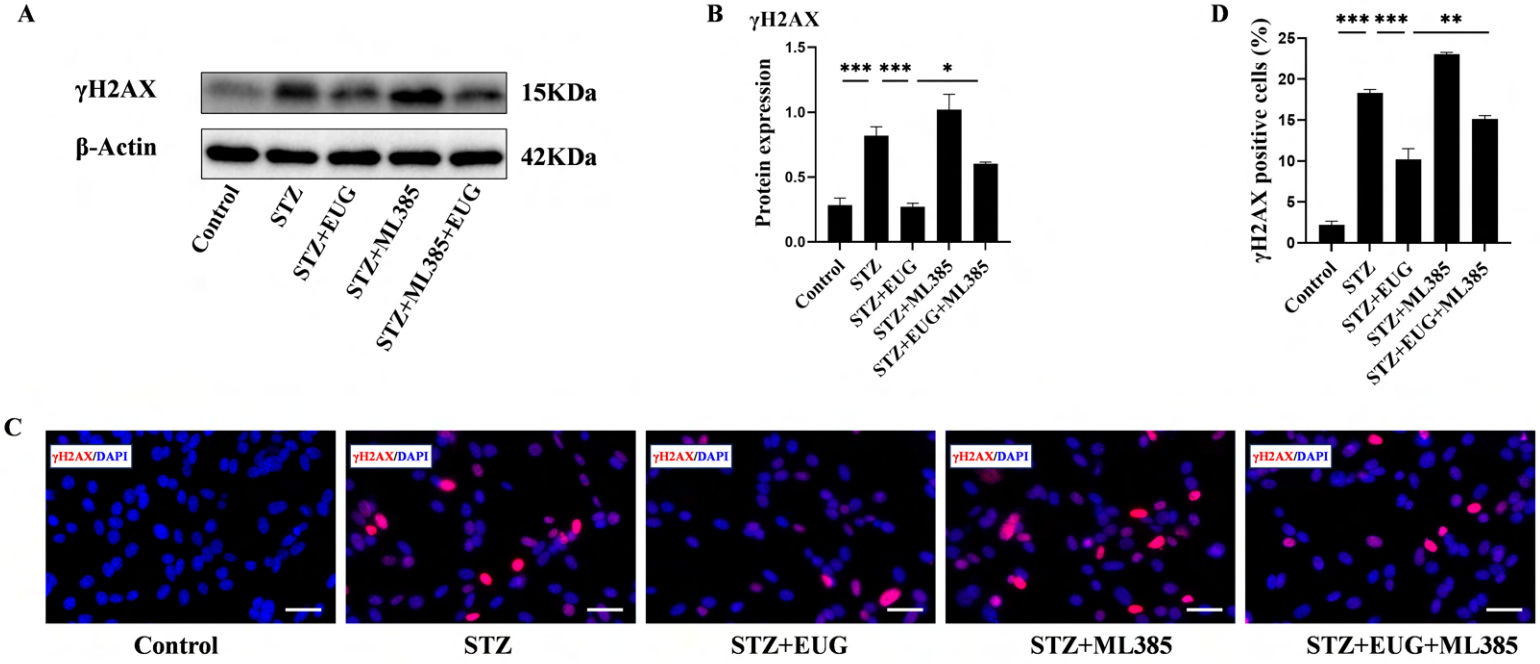
A
γH2AX
β-Actin
15KDa
42KDa
Control
STZ
STZ+EUG
STZ+ML385
STZ+ML385+EUG
B
γH2AX
Protein expression
1.5
1.0
0.5
0.0
***
***
*
Control
STZ
STZ+EUG
STZ+ML385
STZ+EUG+ML385
D
γH2AX positive cells (%)
25
20
15
10
5
0
***
***
**
Control
STZ
STZ+EUG
STZ+ML385
STZ+EUG+ML385
C
γH2AX/DAPI
Control
STZ
STZ+EUG
STZ+ML385
STZ+EUG+ML385

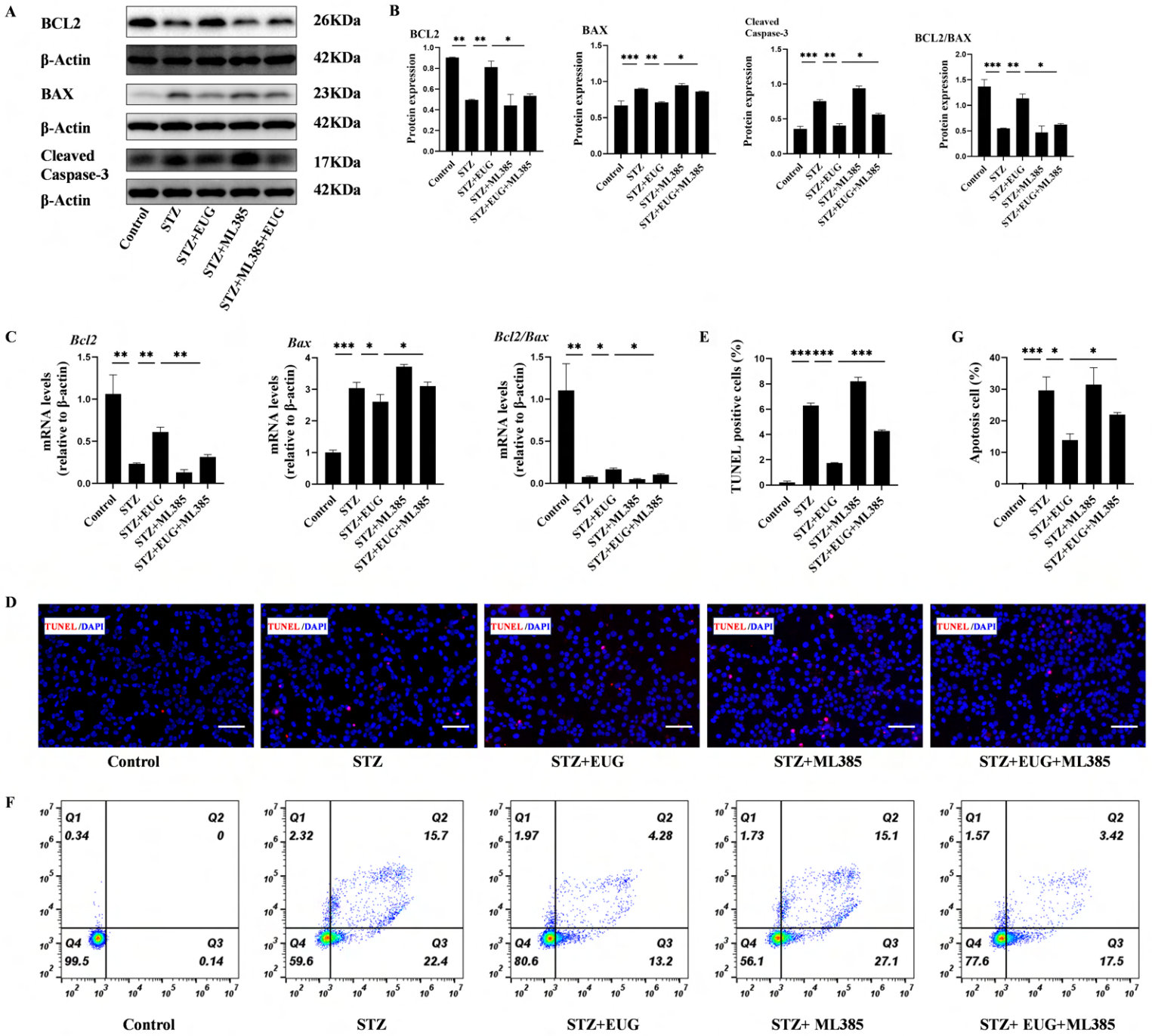
A
BCL2
26KDa
β-Actin
42KDa
BAX
23KDa
β-Actin
42KDa
Cleaved Caspase-3
17KDa
β-Actin
42KDa
Control
STZ
STZ+EUG
STZ+ML385
STZ+ML385+EUG
B
BCL2
BAX
Cleaved Caspase-3
BCL2/BAX
Protein expression
C
Bcl2
Bax
Bcl2/Bax
mRNA levels (relative to β-actin)
E
TUNEL positive cells (%)
G
Apoptosis cell (%)
D
TUNEL /DAPI
Control
STZ
STZ+EUG
STZ+ML385
STZ+EUG+ML385
F
Q1 0.34
Q2 0
Q4 99.5
Q3 0.14
Q1 2.32
Q2 15.7
Q4 59.6
Q3 22.4
Q1 1.97
Q2 4.28
Q4 80.6
Q3 13.2
Q1 1.73
Q2 15.1
Q4 56.1
Q3 27.1
Q1 1.57
Q2 3.42
Q4 77.6
Q3 17.5
Control
STZ
STZ+EUG
STZ+ ML385
STZ+ EUG+ML385

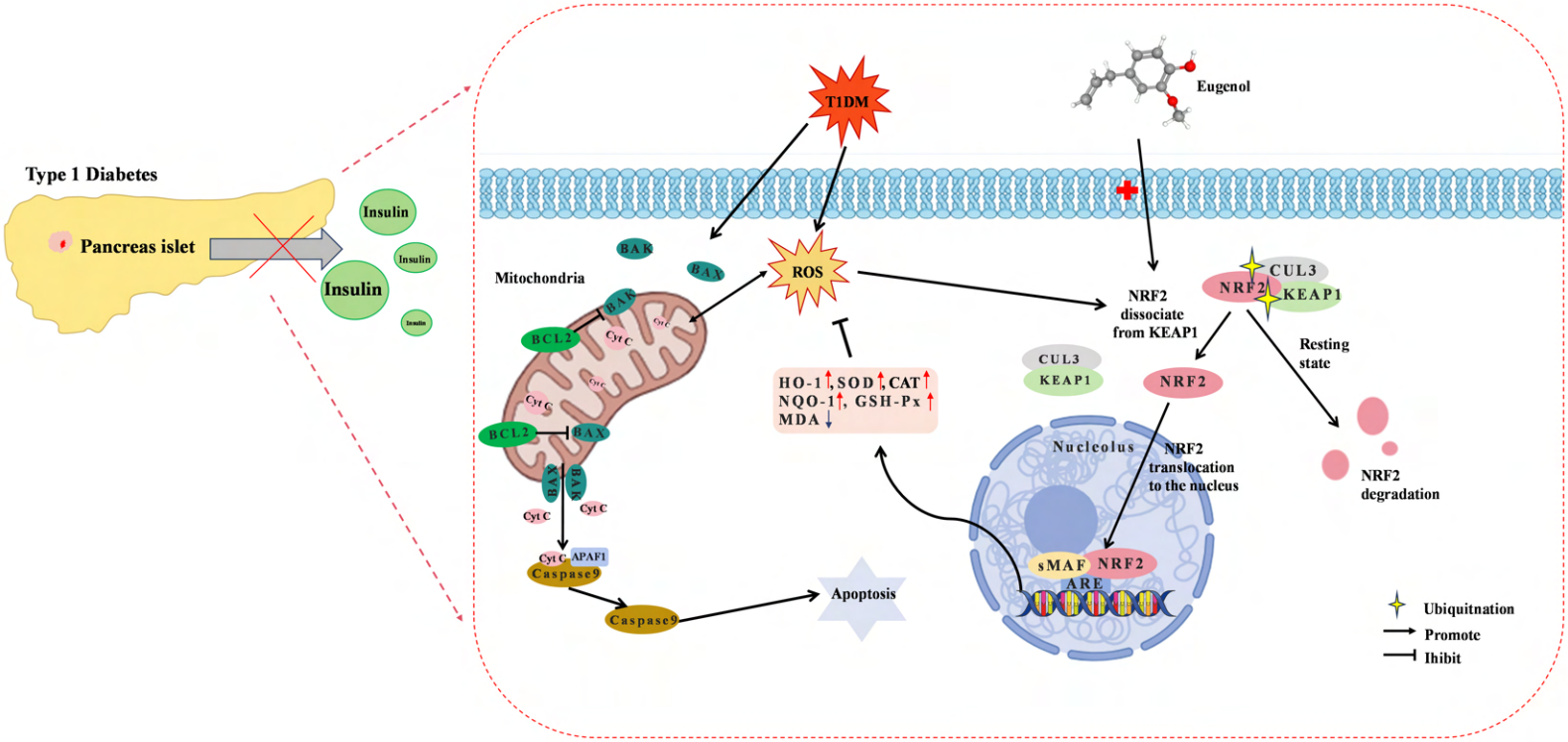
Type 1 Diabetes
Pancreas islet
Insulin
Insulin
Insulin
Insulin
T1DM
Eugenol
ROS
Mitochondria
BAK
BAX
BAX
BCL2
Cyt C
Cyt C
Cyt C
BCL2
BAX
BAX
BAK
Cyt C
Cyt C
Cyt C
APAF1
Caspase9
Caspase9
Apoptosis
HO-1↑, SOD↑, CAT↑
NQO-1↑, GSH-Px↑
MDA↓
NRF2
dissociate
from KEAP1
CUL3
NRF2
KEAP1
CUL3
KEAP1
NRF2
Resting
state
NRF2
degradation
Nucleolus
NRF2
translocation
to the nucleus
sMAF
NRF2
ARE
Ubiquitnation
Promote
Ihibit

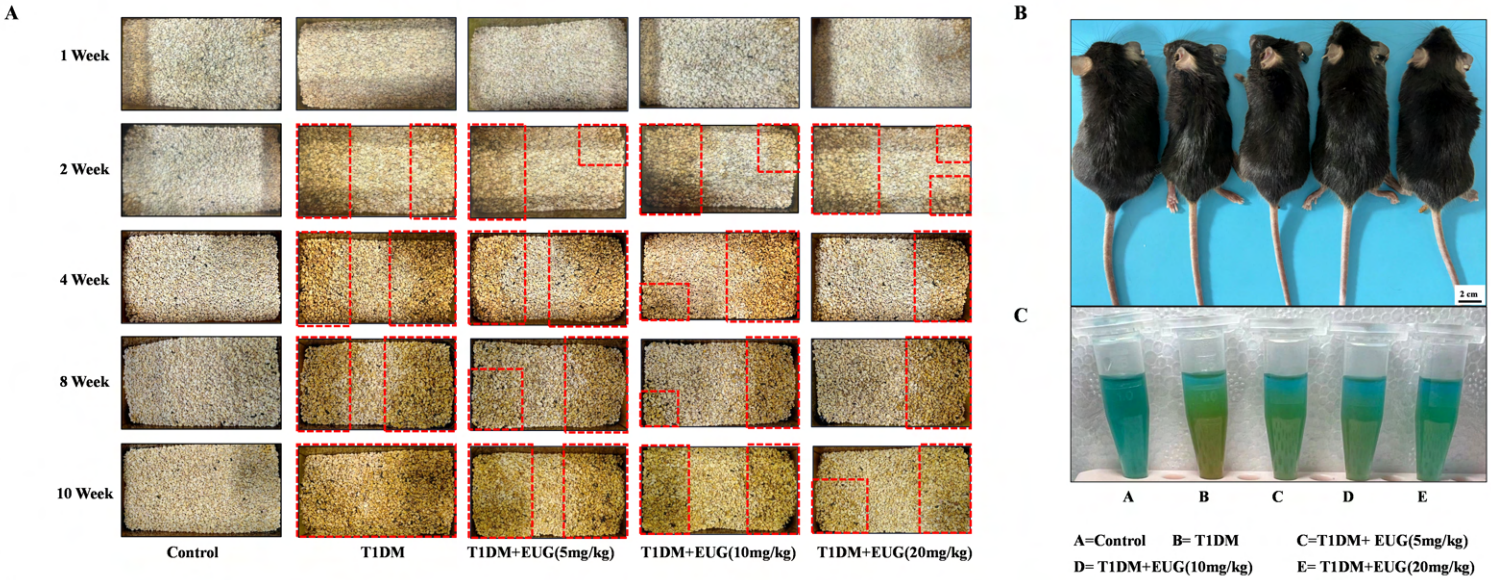
A
1 Week
2 Week
4 Week
8 Week
10 Week
Control
T1DM
T1DM+EUG(5mg/kg)
T1DM+EUG(10mg/kg)
T1DM+EUG(20mg/kg)
B
2 cm
C
A
B
C
D
E
A=Control
B= T1DM
C=T1DM+ EUG(5mg/kg)
D= T1DM+EUG(10mg/kg)
E= T1DM+EUG(20mg/kg)

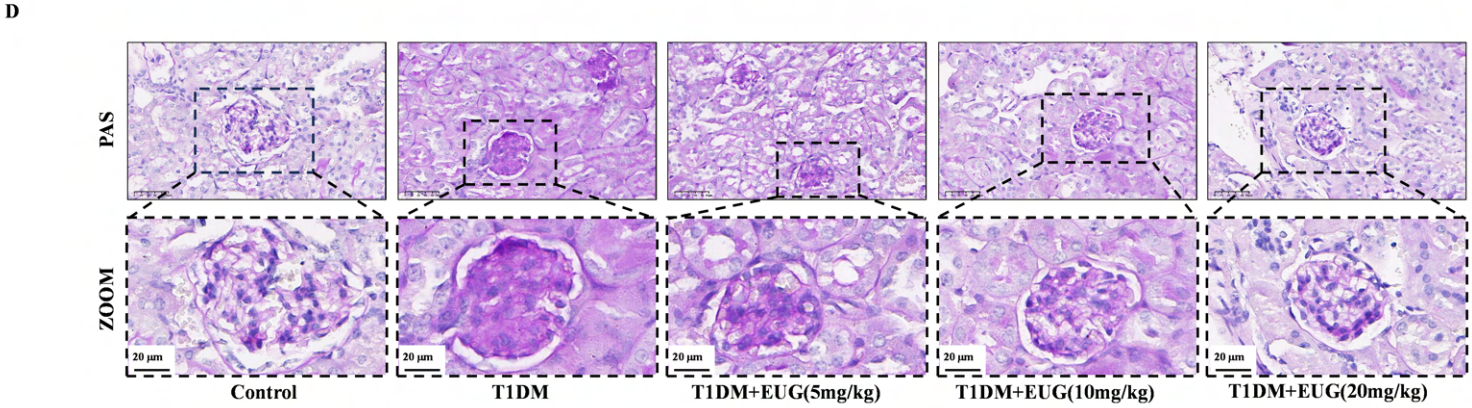
D
PAS
ZOOM
20 μm
Control
T1DM
T1DM+EUG(5mg/kg)
T1DM+EUG(10mg/kg)
T1DM+EUG(20mg/kg)

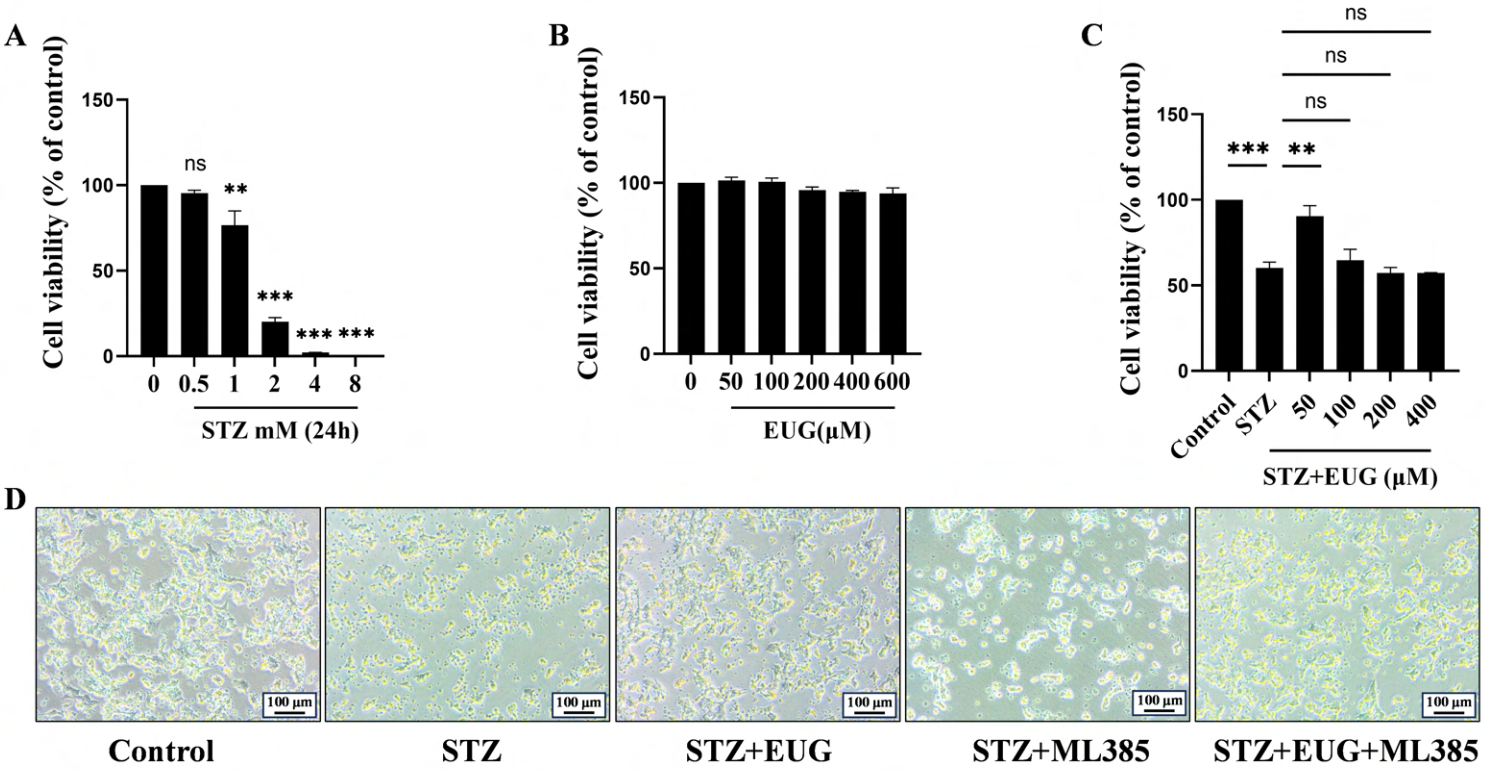
A
Cell viability (% of control)
150
100
50
0
ns
**
***
***
***
0
0.5
1
2
4
8
STZ mM (24h)
B
Cell viability (% of control)
150
100
50
0
0
50
100
200
400
600
EUG(μM)
C
ns
ns
ns
Cell viability (% of control)
150
100
50
0
***
**
Control
STZ
50
100
200
400
STZ+EUG (μM)
D
100 μm
Control
STZ
STZ+EUG
STZ+ML385
STZ+EUG+ML385